DEUTSCHES ELEKTRONEN – SYNCHROTRON

DESY 91-012
March 1991

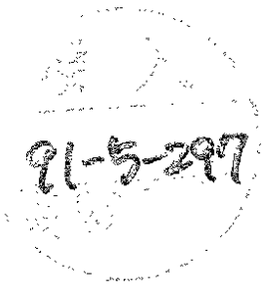

On Neutrons in Uranium-Scintillator Calorimeters
(One Neutron Monte Carlo)

T. Tymieniecka

Inst. of Experimental Physics, University of Warsaw

ISSN 0418-9833

NOTKESTRASSE 85 · D-2000 HAMBURG 52

DESY 91-012
March 1991

ISSN 0418-9833

On Neutrons in Uranium-Scintillator Calorimeters

(One Neutron Monte Carlo)

T. Tymieniecka[1]
Institute of Experimental Physics, University of Warsaw, Warsaw

Abstract

To understand the mechanism of neutron energy deposition in uranium-scintillator calorimeters a fast Monte Carlo code has been developed to simulate the behaviour of neutrons with energy below 20 MeV. The code predictions are compared to experimental measurements. Some comments are drawn on the size of the signal produced by neutrons and their contribution to the energy resolution of uranium calorimeters with hydrogenous readout.

1. Introduction

Many theoretical and experimental studies have been pursued with the aim to improve the energy resolution for a hadron calorimeter. The present Monte Carlo investigation has been motivated by a series of experiments performed as prestudies for the ZEUS uranium-scintillator calorimeter [1].

The fluctuations in hadronic showers come from a large variety of hadronic interactions. A shower in which neutral pions are aboundantly produced has a different energy deposition in space than that without them. Nuclear interactions of hadrons lead to some disintegrations of nuclei, on average larger for baryons than mesons [2]. Considerable differences are expected between hadronic showers with or without a large number of nuclear fragments, as the nuclear processes are strongly correlated with the binding energy loss.

In order to simplify a description of a hadron shower in a calorimeter the shower can be splitted into components [3-8], every one of them characterized by the same general features. Then, for the understanding of some aspects of detection it is possible to investigate the individual component separately. A feature of particular interest for calorimetry is the relation between the energy carried and the recorded calorimeter signal as well as the spatial and time distributions of signals. This paper investigates in detail the part of nuclear component derived from the production and interaction of neutrons with kinetic energy below 20 MeV.

Neutrons are a significant part of the nuclear hadronic component, in particular for neutron-excess materials (high A/Z-ratio). As an example, in multi-GeV proton uranium

[1]/This work is partially supported by Deutsches Elektronen-Synchrotron DESY, Hamburg and the Research Programme CPBP 01.09 and 01.06, Warsaw.

interactions, on average about 30 nucleons are emitted as light nuclear fragments or free nucleons [2]. About a half of them are free neutrons. At 500 MeV about 14 free neutrons are emitted with energy below 12 MeV [2]. Whereas charged fragments deposit their energies close to the interaction point, neutrons, once they have been produced, can travel for tens of centimeters before being absorbed. Those with energy below 20 MeV produce further neutrons and photons in nuclear reactions; a neutron sub-shower is created, which affects only the energy carried by the nuclear components of hadronic showers.

Neutrons themselves do not ionize. Free protons can effectively convert the neutron kinetic energy into energy of charged particles via elastic scatters. In a calorimeter with hydrogenous readout medium the part of the energy carried by the neutron component can be detected. The fraction of the calorimeter signal produced by neutrons depends on the amount of high A/Z nuclei (*the sources of neutrons*) and on the amount of free protons (*the converters of neutron energy into ionization*).

To understand the mechanism of neutron energy deposition it is necessary to follow the neutrons one by one on their way through the calorimeter. Therefore, a special fast Monte Carlo programme, called the **"One Neutron Monte Carlo"** (ONMC), has been developed to simulate the behaviour of neutrons with energy below 20 MeV. The code permits an estimation of the contributions from the different processes and thus allows to determine which effects, out of many, are essential. An earlier version of the code has been used in [3] to investigate detection of hadron showers in uranium-scintillator calorimeters. Some further studies published in [4] are done with NEUKA, the code based on a simplified version of the ONMC routines implemented for use in hadronic shower simulations by FLUKA86[9].

This paper is organized in the following way. Section 2 describes the neutron production. In section 3 the model for transport and interactions of evaporation neutrons with the calorimeter materials is discussed. It mainly concentrates on uranium-organic scintillator composition with a simplified extension to lead-scintillator and to uranium-gases containing some free protons. The gas calorimeters reflect the importance of effects related to the amount of hydrogen in active media. The study of lead-scintillator compositions leads to a better understanding of neutron amplification by fission of uranium. The accuracy of the model and the essential features of the neutron cascade are the subject of section 4. In section 5 the model predictions are compared to experimental results from activation measurements [6] and to calculations done with HERMES [7] and by Wigmans[8]. Finally, in section 6, the detection of neutrons is discussed for the case of the ZEUS uranium-scintillator calorimeter[1]. Unless explicitly stated otherwise:

- the energy is the kinetic energy of a particle;
- the interaction length units, λ, are taken from the Particle Data Booklet [10], however, for all calculations the energy dependent cross sections are taken;

- calorimeters are of the sampling type with alternating layers of absorber and readout material.

2. Evaporation Neutrons

In the traditional description of an interaction between a high-energy hadron ($E_{kin} \geq O(100)$ MeV) and a nucleus two stages can be distinguished: a fast intranuclear cascade followed by a slow deexcitation process of the remaining nucleus. For the high A/Z materials the deexcitation goes through an evaporation process competing with high-energy fission. Both lead to the emission of free nucleons, nuclear fragments and nuclear photons. Each of the interactions is a point-like source of neutrons, which are called here evaporation neutrons.

The available experimental data on neutron production from heavy nuclei are rather limited and inadequate, in particular as far as such essential properties as the total neutron yield, the energy spectrum or the angular distribution [11-13] are concerned. Several theoretical investigations have been carried out to understand processes in uranium and in lead needed for nuclear reactor calculations[12]. Some of our assumptions are based on results of these approximations when no detailed information from measurements is available.

The probability $\Phi(E_n)$ of emission of an evaporation neutron with energy E_n, is described by the Weisskopf statistical theory leading to an energy spectrum of neutrons given by $\Phi(E_n) \propto E_n \cdot \exp(-2E_n/\bar{E}_n)$. The average kinetic energy of the neutrons $\bar{E}_n$, emitted from sources created by nucleons of a few hundred MeV on uranium and lead, is measured to be equal to 3.6 MeV and 3.4 MeV, respectively [11]. For hadron interactions at higher energies the mean neutron energy is still about the same, about 3.55 MeV for uranium and lead [7]. At the lower energies the mean energy of evaporation neutrons from lead decreases to about 2 MeV for 30 MeV incident protons. The decrease reflects a diminishing probability for high-energy fission. More information on experimental neutron spectra can be found in [11].

The Weisskopf formula is not completely adequate (see e.g. Brückmann et al., [7]). The deviations are due to the motion of the evaporating nuclear fragments, which recoil after the internuclear cascade and/or fission. Taking into account this effect in the present studies it is assumed that evaporation neutrons are emitted isotropically from a point-like source and have a Maxwell energy spectrum,

$$\Phi(E_n) \propto \sqrt{E_n} \cdot \exp(-E_n/T)$$

with a maximum energy of neutrons equal to 20 MeV. The temperature T expresses the average kinetic energy of the neutrons according to $T=2/3 \cdot \bar{E}_n$. The average energy is taken to be equal to 3.55 MeV for most of the studies. It is valid for neutrons from interactions of

hadrons with energy above 50 MeV on uranium, and above 1 GeV on lead. For the latter, as mentioned, the average energy depends on the incoming energy of hadron. Therefore, the spectrum of evaporation neutrons of 2 MeV for lead, as a lower limit, is also the subject of further investigations. The spectra are presented in fig.1.

The number of evaporation neutrons produced in hadron showers scales approximately with the energy of the showering particles E_h like $42 \cdot (E_h/1GeV)^{0.88}$ in uranium. The formula is obtained from the studies of hadron showers of energy between 10 GeV and 100 GeV in the ZEUS uranium-scintillator calorimeter [3] and is in agreement with estimate given in [7] and [14].

The neutron yield for lead is roughly 2/3 that of uranium for 10 GeV hadron induced showers[7], and 1/3 for 600 MeV proton-induced showers[6]. It reflects the fast decrease of the probability for the fission of lead below 1 GeV.

An additional source of neutrons in hadronic and electromagnetic showers which is not considered in this paper, is photoproduction. The main contribution to photoneutron yields comes from the giant dipole resonance region ($6.1MeV \leq E_\gamma \leq 20MeV$), with a cross section for neutron emission from uranium of about 0.5 barns at $E_\gamma \approx 14MeV$. The average kinetic energy of photoneutrons is higher then for evaporation neutrons[15].

3. Model of Neutron Interactions

In this section our assumptions on the modelling of the neutron interactions ($E_n \leq 20MeV$) with nuclei are described. They are essentially based on experimental results.

Calorimeter materials are usually a mixture of isotopes like uranium or compound materials like scintillators. The model deals only with the pure isotopes of ^{238}U, ^{12}C and ^{1}H, and with natural lead[2]. Organic scintillators as well as hydrogen containing gases are assumed to be a mixture of carbon and hydrogen with relative ratios and densities as given in the Particle Data Booklet [10].

An evaporation neutron initiates a neutron cascade composed of neutrons. A neutron can undergo several reactions with **uranium**: elastic and inelastic scattering, fission, (n,2n), (n,3n) processes and capture. The cross sections [16] for these interactions are presented in fig. 2. To give a feeling for the spatial spread of the neutron cascade we note that the mean free path of 2 MeV neutrons for elastic interaction in pure uranium is 4.7 cm; it is 7.8 cm for inelastic scattering and 38 cm for fission. The mean free path of neutrons is relatively large compared with the calorimeter layer thickness (typically, <1cm). The neutron-uranium interactions are simulated as follows.

[2]/Natural lead consists of four isotopes ^{204}Pb, ^{206}Pb, ^{207}Pb, ^{208}Pb with relative abundances, 0.01, 0.24, 0.23, 0.52, respectively. The three heavier isotopes are end products of the naturally occurring radioactive chains. Thus, their amounts in particular samples vary within a few percent.

- Neutron elastic scattering on uranium is described by a coherent elastic model above 1 MeV neutron energy and classical elastic scattering, i.e. 2-body kinematics and isotropy in space, below 100 keV. For the coherent elastic process a neutron momentum transfer is defined by the semiempirical formula proposed by Ranft and Routti [17]. The forward peak in the angular distributions observed in experimental data on the process [18,19] is reproduced. The assumption of the coherent elastic model leads to a negligible change of the neutron direction and to a small fractional energy loss of about 1/300 per scattering. Below 1 MeV an increase of an isotropic component in the experimental angular distributions is observed. To simulate it two-body kinematics with isotropy in space is taken, if no solution to the kinematical equations is found for the momentum transfer sampled from the coherent-elastic formula. The forward peak decreases faster than in the experimental data. Below 100 keV the process is described by isotropy and 2-body kinematics with the relative mean energy loss of about $2A_U/(A_U+1)^2 \approx 2/238$. It does not agree with the experimental observations where an anisotropy is still detected at 75 keV [20].

- Neutron-induced fission of uranium produces on the average 2.6 neutrons. The neutron energies E_n, are sampled according to a Maxwell distribution, discussed before, $\Phi(E_n) \propto \sqrt{E_n} \cdot \exp(-E_n/T)$ [21]. Discrepancies between a Maxwell distribution and the experimental spectra [22] as observed in the energy region below 50 keV and above 15 MeV have been corrected to reproduce the latter. The mean number of fission neutrons (called nubar) and their temperature, T, depend on the energy of the incident neutron, E_0, in agreement with the experimental data [21]. Nubar is taken from the table of the mean values up to a neutron energy of 6 MeV [23] and above 6 MeV from a linear dependence of nubar=$0.145*E_0+2.35$. The actual number of fission neutrons is chosen randomly from a Poisson distribution with the average value being nubar. The temperature is taken to be 1.33 MeV near the threshold increasing linearly at the rate of 0.02 MeV/MeV. The fission neutrons are emitted isotropically in the laboratory frame [24].

- Neutron inelastic scattering on uranium depends strongly on energy. For the low energy neutrons ($\leq$ 2.5 MeV) the amount of energy lost by a neutron is calculated from the nuclear level excitation model. In this model the neutron excites one of the uranium levels and loses the corresponding level energy. The probability of an excitation and a neutron energy transfer are calculated according to Sheldon et al.[25] and Hogdsen et al.[26]. The assumed neutron angular distributions are anisotropic only at low energy transfers, below 1 MeV. The process is dominated by an excitation of the lowest states, in particular the 45 keV and 145 keV levels, still contributing at 3.4 MeV[19]. Therefore, the average energy loss by a neutron is small. For example,

according to Sheldon's model a 2 MeV neutron loses about 550 keV per interaction leaving still enough energy for the neutron to create a secondary fission.

In the higher energy region, above 6 MeV, the statistical model of the excited nucleus is used. It assumes that the neutron merges with the nucleus and forms a compound nucleus which then evaporates one, two or three neutrons isotropically. The evaporation spectra of the second and third neutron are described by the phenomenological distribution given by Craner et al.[27], while the one for the first emitted neutron is defined in terms of a density level parameter of uranium. No correlation in energy or space between the sequential neutrons is assumed here. The number of evaporation neutrons is determined by the inelastic, (n,2n) and (n,3n) cross sections of fig.2. Although these processes lead to a multiplication of neutrons, the main effect is a degradation of their energies, mainly below 1.5 MeV, into a region with low fission probability. Frequently, the neutron energies are below the threshold for fission, i.e. 0.5 MeV. For a 14 MeV neutron the mean energies of the sequential emitted neutrons are 1 MeV, 1.13 MeV and 0.36 MeV, respectively.

The model for the first neutron emission is extended to a lower energy region, below 6 MeV. The evaporation spectrum corresponds to a Maxwellian one with a mean energy of the emitted neutrons of about 20% of the incoming neutron energy[26,16]. Thus, in the region between 2.5 and 6 MeV it is assumed that inelastic scattering occurs as a mixture of the above two models, the statistical approach and the nuclear level excitation model. The relative contributions are parameterized in a form of a probability that the inelastic scattering happens according to the model: at 2.5(6.1) MeV the probability is 1(0) for the level excitation process and 0(1) for the statistical process; in between 2.5 and 6.1 MeV these probabilities vary linearly with energy.

- Neutron capture in uranium leads to an excited state of ^{239}U, which subsequently decays to the ^{239}U ground state by the emission of a series of photons carrying away, in total, an energy of at least 4.8 MeV. In the model the neutron disappears without any further consequences. This process is very important for neutrons with energies below 10 keV and dominates the neutron cascade below 0.1 keV. Therefore neutrons are followed down to an energy of 0.4 eV where they are assumed to be captured in the nearest uranium nucleus.

A similar model is proposed to describe the neutron interactions in **lead**. The main difference between uranium and lead is the lack of neutron-induced fission for the latter and drastically different cross sections for the other processes (fig.3). The features of naturally occurring lead are dominated by the doubly magic isotope 208. Its first excited state is at 2.615 MeV and the next one at 3.198 MeV to be compared with 45 keV and 145 keV for ^{238}U or 0.8 MeV and 1.17 MeV for ^{206}Pb. That explains the small cross section for neutron

inelastic scattering on natural lead below 3 MeV. The low density of excited states for lead is reflected also in the level density parameter of the nuclear statistical model, which is nearly three times smaller for nuclei around A=208 than for those around A=238. The probability for neutron capture on ^{208}Pb is approximately zero. The binding energy of the neutron for all lead isotopes is higher than for ^{238}U. The thresholds for multiplication processes in lead via (n,2n) and (n,3n) are assumed to be 1.3 MeV and 2.6 MeV above the ones for ^{238}U. Therefore, a neutron in lead travels relatively far without any deposition of its energy. The mean path of a 2 MeV neutron in natural lead is 5.5 cm for elastic scattering, 50 cm for inelastic scattering and 19 meters for n-capture. For this reason the Pb-model has to be more than a simplified "uranium-without fission" model.

The neutron interactions considered by the model are elastic scattering, inelastic scattering, (n,2n) and (n,3n) processes and neutron capture. They are governed by the natural lead cross sections (fig.3) with the mean atomic number and density of lead. The main assumptions are the same as for uranium. The elastic scattering and neutron capture process[3] are described by the same algorithms as for the U-model. However, in contrast to uranium, neutrons below the cut-off energy of 0.4 eV, are assumed to be captured on hydrogen or lead according to the relative probabilities at this energy. As in the case of uranium, inelastic interaction of a neutron with an energy above 7.4 MeV yields the sequential emission of one, two or three neutrons. The spectra of the outgoing neutrons are calculated according to the statistical model of the excited nucleus[27]. The spectrum of the first emitted neutron is defined by the density level parameter of lead. The spectra of secondary neutrons are identical to the ones used in the U-model, but calculated with respect to lead thresholds. Thus, for an incoming neutron of 14 MeV, on the average 1.43 MeV of the energy is carried away by the first neutron and 0.95 MeV of energy by the second one. Features of n-Pb interactions for the neutron energy below 5.5 MeV change significantly from one isotope to another. For nuclear excitations below 3.2 MeV [28] a neutron momentum transfer is defined by the measured differential cross sections weighted according to the relative abundance of lead isotopes. The probability of an excitation at higher energy is calculated from the statistical model without spin or parity effects and temperatures adopted as for natural lead. In the region between 5.5 MeV and 7.5 MeV, in analogy to the U-model, the contribution from the statistical model increases linearly. This approach, although very crude compared with the detailed U-model, is in agreement with the experimental data [29].

In the organic **scintillator** a neutron undergoes mainly elastic interactions with its components: hydrogen and carbon. The mean free path of 2 MeV neutrons is 6.6 cm and 11.8 cm, respectively, comparable to the values in uranium and lead. The cross sections for

[3]/Energy released in form of nuclear photons is 3.9 MeV for ^{208}Pb, 7.4 MeV for ^{207}Pb, 6.76 MeV for ^{206}Pb and 6.7 MeV for ^{204}Pb.

the interactions in hydrogen and carbon are given in fig. 4. The interactions are simulated as follows.

- Neutron scattering on hydrogen. The energy loss of a neutron is calculated according to the 2-body kinematics and angular isotropy. The neutron transfers on average half of its kinetic energy to the recoiling proton, which then produces an ionization signal. In addition, the neutron capture into deuteron is considered although the process is only important for eV-neutrons.

- Neutron interactions with carbon. The elastic, inelastic and absorption processes are simulated according to their cross sections. In inelastic scattering only the excitation of the 4.3 MeV level is considered and subtracted from the incoming energy. The energy loss for elastic(inelastic) scattering is determined from the 2-body kinematics assuming isotropy in space. Neutrons are absorbed without any further consequences.

The calorimeter **signal** is determined by the amount and density of the energy deposited in the readout material. The contribution to the signal originating from the energy loss of neutrons by scattering is called the neutron signal.

Materials containing hydrogen convert the neutron kinetic energy into energy of recoiling protons efficiently. However, for scintillator due to a saturation effect the light yield produced by the highly ionizing protons is not proportional to the energy deposited. A similar effect, although less pronounced, is observed in gas chambers. The relation between the relative collected light, L/L_o, and the energy loss, dE/dx, is parameterized according to Birk's formula

$$\frac{L}{L_o} = \int \frac{dE/dx}{1 + k_B/\rho \cdot dE/dx} dx,$$

where ρ is density of the medium. dE/dx is taken from [30] up to proton kinetic energies of 7 MeV for scintillators, while up to 0.2 MeV for gases, explicitly for methane CH_4 and isobutane C_4H_{10}. Above these values an approximation of the Bethe-Bloch formula is adopted up to 20 MeV. For all the studies presented here, the material dependent parameter k_B for scintillator is taken to be that of the scintillator of SCSN38, k_B= 0.0085 $g/(MeV \cdot cm^2)$ [1], and one half of it for gaseous readout. The saturation causes a strong suppression of the contribution to the signal from the lower energy recoiling protons. To stress the importance of the effect we mention that in scintillators the ratio L/L_o is 28%, if the energy of a 2 MeV proton is transformed into measurable light and 12% for a 0.1 MeV proton. For a typical evaporation neutron this factor is less than a quarter of the total energy transferred to recoil protons.

The finite size of the scintillator plates is taken into account by transporting protons in 1 MeV steps. The light generated by recoiling protons below 1 MeV is added to the neutron signal irrespective of their position in the readout material. This introduces a

negligible overestimate of the signal for scintillator thickness above a few milimeters which however, increases for thinner layers of the active medium (spaghetti calorimeters) or for less dense ones(gaseous readout).

The energy deposited in the scintillator by a recoiling carbon nucleus or any other nuclear fragment from carbon or uranium is not converted into light. Nuclear photons, abundantly produced in each of the described types of neutron interactions (inelastic, capture, fission, C-fragmentation) are also not considered. It has to be stressed that at least three quarters of the nuclear photons in hadron showers originate from neutron interactions. Some details on the nuclear photon contribution to hadron showers can be found in [7] and [8]. Thus according to [7] a few percent of nuclear photon energy contributes to the signal in the conventional scintillator-uranium calorimeters.

4. Neutron Cascade

In the previous section a detailed description of the assumptions of the model has been given. The aim of this section is to show (i) the essential characteristics of the neutron cascade development and (ii) how uncertainties in the model assumptions reflect on the calculation of the neutron cascade features and the detected signal.

The enhancement of the pure hadron response and the recuperation of the binding energy losses to achieve compensation make the neutron detection important. Also, due to the large mean free path of neutrons, they give an additional spread to the lateral and longitudinal profiles of hadronic showers, and therefore an additional energy leakage. Even a small fraction of the neutrons, which leak through the walls of a calorimeter, might give rise to a major problem for any electronics installed nearby. A decrease of angular resolution and/or an increase of background from unwanted signals created in the other detectors surrounding the calorimeter is expected. Any additional detector inside the calorimeter such as silicon diodes may suffer from neutron induced radiation damage.

The neutron signal, as defined in the previous section is represented quantitatively by:

- the fraction of neutron energy transferred to free protons (or its equivalent signal, called the sampling fraction);
- the number of neutrons involved in a neutron-induced cascade, called n-flux, described by the number of n-captures (or proportional to the number of n-induced fissions for uranium);
- the time, t^{signal}, when 90% of the signal is recorded;
- the lifetime, $t^{n\ capt.}$, of a neutron induced cascade defined as the time interval between the emission of the evaporation neutrons and 90% n-captures;

- the radius of a circle around the neutron source in the sampling layer plane, R_{XY}^{signal}, containing 90% of the calorimeter signal; it defines the angular resolution;
- the radius of a circle around the neutron source in the sampling layer plane, $R_{XY}^{n\ capt.}$, containing 90% of neutron captures inside (or R_{XY}^{fiss} for fission); it defines the spread of the n-flux.

These features depend on:

- the energy of an evaporation neutron;
- the geometry of the calorimeter, i.e. its lateral and longitudinal size, thickness of absorber plates, d_{abs}, thickness of scintillator plates, d_{Sc}, gaps between the plates, amount of dead material, or extra materials and their physical properties.

The dependence on the neutron spectrum originates from the energy dependence of the cross section of the different neutron processes (figs 2-4); the sensitivity to technical details of a calorimeter is due to the long mean path of neutrons before they disappear. Therefore the features of the simulated neutron cascades are very sensitive to the model parameters.

To illustrate features of the neutron cascade, calculations have been done for an infinitely large block of absorber, for a ZEUS-type but infinitely large calorimeter (d_{abs}=0.33 cm, d_{Sc}=0.26cm) [1] and for a calorimeter where the thickness of the absorber plates is increased by a factor of three compared to the ZEUS-type calorimeter. Sources of evaporation neutrons are assumed to be situated uniformly along the depth of the absorber plate to avoid local effects. Evaporation neutrons are sampled from the Maxwell energy distribution discussed before with a mean energy of the neutrons of 3.55 MeV, if not stated otherwise. The calculated number of interactions and mean energy losses per evaporation neutron are summarized in Table 1 for uranium as absorber and in Table 2 for lead as absorber with and without scintillator as detector. For gaseous readout the results are presented in Table 3. In addition, for every material composition an effective collision length A_{coll}^{eff}, and an effective interaction length A_{int}^{eff} are given. They are defined as an average distance between a neutron source and the first collision (interaction) of evaporation neutrons.

A few remarks are in order. A massive absorber block is equivalent to a sampling calorimeter interspersed with thin silicon detectors. A uranium calorimeter with 0.33cm thick absorber and 0.26 cm scintillator plates is compensating [1]. Also a calorimeter with 1.0 cm lead plates and 0.26 cm scintillator plates is close to a compensating calorimeter [31].

4.1 Uranium/Scintillator

According to the calculations (Table 1) the multiplication factor of an evaporation neutron, as defined by the number of n-captures, is 1.38 for the ZEUS-type calorimeter, whereas it

is 1.77 for massive uranium. Only one-sixth and one-third of the evaporation neutrons, respectively, lead to fission. Thus, hydrogen damps the development of the neutron cascade.

Neutrons on average undergo many elastic scatterings on uranium but loose only a tiny amount of energy. The process is dominated by scattering of neutrons with energies below 0.5 MeV; the number of scatters as well as the spread of n-captures is very sensitive to the assumed energy limit, to which neutrons are followed in the cascade. We use 0.4 eV. In the Monte Carlo programme a neutron undergoes about 80 scatters before being captured. Even a slightly inadequate description of the process may lead to a significant effect after a series of sequential repetitions. Therefore, it is important to understand the limitations of the proposed model. Again, the infinite ZEUS calorimeter is considered (i) with a Maxwell spectrum of evaporation neutrons, and (ii) with a monoenergetic source of neutrons[4]. The parameters of the model are checked by varying them within the uncertainties. Results per evaporation neutron are presented in fig.5 with the shaded area indicating the extent of uncertainty. Some of the contributing uncertainties are as follows.

- For the **fission** process many formulae have been proposed to describe the energy dependence of the number and energy spectrum of fission neutrons [18,22,23]. The variation of the predicted number of n-captures is within 11% and the number of fissions within 5%.
- For **elastic** scattering an enhancement of the anisotropic component does not change the amount of energy deposition and changes only weakly its spatial distribution, R_{XY}^{signal}, which varies by 2 cm for different assumptions. It affects the spatial distribution of n-captures by 4 cm.
- In the **inelastic** process on uranium a neutron loses a substantial part of its energy (Table 1); the amount is very sensitive to the model assumptions for the process. An increase of the number of neutrons, and therefore their energy transfer to free protons, is suppressed if a neutron falls below the fission threshold due to a large loss of energy. Since the inelastic cross section is considerably larger than the fission cross section, it prevents neutron proliferation in uranium calorimeters. The uncertainty of the inelastic scattering description is the main contribution to the shaded area in fig. 5.
- In neutron multiplication via the **(n,2n), (n,3n)** process, as in inelastic scattering the energies of the emitted neutrons determine their further 'fate'. However, only 5% of the evaporation neutrons have an energy $E_n \geq 10$ MeV. Their contribution is unimportant; in particular the contribution of the third neutron in the (n,3n) process to the energy deposition is negligible.

[4]/Neutrons of 1-6 MeV cover the essential part of the Maxwell spectrum (fig.1).

We conclude that, although for a monoenergetic source of neutrons the uncertainty of the energy deposition can reach up to 15%, the estimation of the detection efficiency of an evaporation neutron from a Maxwell spectrum has an uncertainty of less than 10% due to the model parameters. With a similar accuracy one could study the behaviour of photoneutrons.

An evaporation neutron travelling through the calorimeter produces other neutrons through fission or neutron multiplication processes ((n,2n) or (n,3n)). By scattering in the scintillator, the neutrons create on average 10 recoil protons, although in individual cases more than 100 recoils may take place. The neutron signal is collected from all recoiling protons. The dominant transfer of evaporation neutron energy happens through the first n-p scatter. Thus 57% of the signal is generated in the first scattering while due to fission the next part (up to 90%) during the 17 scatters that follow.

4.2 Lead/Scintillator

The neutron cascade in lead is dominated by elastic scattering (see Table 2). The signals are slightly larger in size, longer in time and more spread in space than the ones in the similar uranium calorimeters. In the lead compensating calorimeter 90% of the signal is created within the first three scatterings. The scatterings that follow, slow down low-energy neutrons to thermal energies. Then they leak out or are captured predominately in ^{207}Pb, and for sampling calorimeters also in hydrogen. We want to stress that the lateral spread of the calorimeter signal, R_{XY}^{signal}, in terms of Λ, is the same $\sim 1.7\Lambda$, for the uranium and lead compensating calorimeters.

Due to the small cross section for inelastic scattering and n-capture in lead below 3 MeV of neutron energy the lifetime of a neutron cascade $t^{n\ capt.}$ is longer than in uranium. Whereas 90% neutrons are captured in uranium after 0.4 μs, for lead calorimeters the 90% neutron absorption happens after 8 μs for 0.33 cm thick absorber layers and about 15 μs for 1 cm thick layers.

As for uranium, the accuracy of the simulation of the neutron processes is predominately determined by the accuracy of the description of inelastic scattering. The experimental differential cross sections used to calculate the neutron energy loss and the relative abundance of lead isotopes give an uncertainty of about 10%.

A large uncertainty originates from the secondary neutron spectra from (n,2n) and (n,3n) processes. The processes which are unimportant for uranium, are the only ones which cause multiplication of neutrons in lead. They reduce the neutron energies to a point where n-scattering on hydrogen become highly probable. The low probability for inelastic scattering and absorption below 2.5 MeV leads therefore to a high probability of the deposition of the total neutron energy in the scintillator material. The uncertainty in the description of the neutron multiplication processes becomes important only for neutrons

of an energy above 8 MeV, like photoneutrons; it is not important for the evaporation neutrons, discussed here.

4.3 Uranium/Hydrogenous Gases

The performance of a uranium calorimeter with gas detectors has been investigated experimentally [32]. The calorimeter response to pions depends strongly on the hydrogen content of the gas. An equal average response for pions and electrons can be obtained but without an improvement of the calorimeter energy resolution with respect to the studies non-hydrogenous readout. In hydrogenous gases the measured signal of hadrons has large non-Gaussian fluctuations which are not observed otherwise.

Results of the simulation of a 0.33cm U-plate calorimeter interspersed with 0.66cm gaseous media are summarized in Table 3. The values are quoted for the important processes only. The densities of hydrogen in gas detectoe is at best three orders of magnitude smaller than for scintillators. Therefore, the neutron cascade develops like that in a massive uranium block. The number of fissions or scatters, the amount of the energy loss as well as the neutron multiplication factor are comparable for both cases. However, the spatial spread increases enormously due to the low fraction of hydrogen and a low density of the medium. This result in a leakage of neutrons. Only 41% of the evaporation neutrons give a signal for the C_4H_{10} calorimeter and 23% for the CH_4 one to be compared with 97% and 99% for the compensating scintillator calorimeter of uranium and lead, respectively. In fig.6 the signals per evaporation neutron are compared. The mean signal for the detected neutrons is two orders of magnitude smaller than in the scintillator calorimeters but still large in comparison with minimum ionizing particles, which deposit 4keV per the 0.66cm thick layer of isobutane. As a result the neutron signal in hydrogenous gases is infrequent but large, and thus a subject to big fluctuations. The spatial spread leads to a significant leakage of neutrons from a typical 50x50 cm^2 test calorimeter[32,33].

The accuracy of the simulation is limited by the same features as for the uranium-scintillator calorimeter.

4.4 Time and Spatial Distribution of Signal

The mean free path of neutrons between subsequent hydrogen elastic scatterings varies strongly with neutron energy, see figs 2-4. This reflects upon a spread of the neutron signal in space, (fig.7) and in time (fig.8). As the neutron travels away from the source its energy decreases. The mean energy of 3.55 MeV at the source drops to 1.4 MeV at the distance of 6 cm in the uranium scintillator compensating calorimeter. More than 3 cm away from the source, the signal is created by a series of small depositions strongly damped by light saturation. In thicker absorber plates, fig.8, slow neutrons deposit their energy later and further away from the source due to an increase of their path length.

The large path length for energy deposition is visible in the spread of the signal in the isobutane-uranium calorimeter (fig.7).

To get a good estimate of the signal it is not necessary to follow neutrons down to thermal energies. A cut-off value of 10 keV is sufficient to collect 98% of the created signal in the uranium compensating calorimeter. But a lower value is advised if a signal faraway from the source which comes from the low energy neutrons, is investigated.

A quantitative measure of the neutron spatial spread in the sampling layer plane can be defined by the radius R_{XY}, of a circle with 90% containment of a process (Table 1-3 and fig.9). Thus, the neutron cascade develops inside a volume of about 20 cm radius, which is slowly increasing with the thickness of the uranium plates. While for lead, the small cross section for neutron inelastic scattering below 3 MeV leads to a wide spread, in particular for n-captures. Keeping in mind the limited accuracy of the n-capture estimates, one notes that 90% of the n captures are inside a 25 cm circle, for U-plate of 2.6cm whereas in lead about 54 cm. The lack of hydrogen causes the large value of R_{XY} and leakage (Table 2) for massive lead.

The spread of the neutron cascade is independent of the direction, even the extreme cases of the directions perpendicular and parallel to the absorber plates. Thus the uranium (lead) calorimeter with 0.26 cm scintillator plates can be considered as a homogeneous mixture of uranium(lead) and scintillator as far as the neutron calculations are concerned.

5. Comparison of the ONMC Predictions with Similar Calculations and Experimental Data

Studies of the energy deposition by hadronic showers including the neutron contribution have also been done elsewhere[7,8,35]. These calculations based on the DYMO [36] and MORSE [37] codes are checked against similar estimates from the ONMC model discussed. The results are in agreement within errors.

The ONMC predictions for the spatial distribution of n-capture and fission products are compared to results from an activation study of a massive uranium block after irradiation with a 591 MeV proton beam.

The experiment done by Leroy et al. [6] is based on the measurements of the induced γ and β-intensity about 3 days after the exposure. Some of the β and γ-rays are attributed uniquely to the decays of certain radioactive isotopes on the basis of their decay period and their energy, i.e. ^{239}Np, ^{103}Ru, etc. The isotopes are products of a number of well defined nuclear processes in p-induced shower. Their abundance estimated via the intensity of the radioactivity, permitted the authors to determine the number of n-captures and fissions at different positions within the uranium block.

Our assumptions for these nuclear processes are:

- ^{239}Np production comes only from the n-capture process $^{238}U(n,\gamma)^{239}U$ followed by β-decays;

- the detected fission products ^{103}Ru, ^{131}I, ^{140}Ba are, in nature, emitted with different frequencies in p-induced fissions and n-induced fissions; in the simulation they are assumed to come from all fission processes with the same probability;

- the high-energy fission process probability is defined by the energy dependent experimental cross sections;

- a heavy spallation product is emitted for every interaction above 30 MeV except fissions or elastic scatterings.

In the simulation the uranium stack is identical to the one used in the experiment. It is composed of 134 U-plates with 0.3 cm thickness and the lateral dimensions of 20 x 120 cm^2. For studies of sampling calorimeters the U-plates are interspersed with 0.25 cm thick scintillators. Also,the infinitely large setups defined as 200 x 200 x 400 cm^3 are simulated to understand differences between raw data and the data corrected for leakage. The beam is assumed to enter perpendicularly to the front U-plate and to go through the middle of it. The radioactivity is assumed to be collected within a cylinder of 2 cm diameter around a line of interest. For more details on the origin of detected processes and the experimental set-up the reader is referred to [8].

The first check of ONMC is based on the measured spatial distributions of spallation products. It is assumed that the sources of evaporation neutrons created by spallation or p-induced fission are distributed in space in the same way as the spallation products. With this assumption we obtain a good description of the transverse distribution of n-capture products and of fission products measured at a depth of 0.6Λ. However, the calculated longitudinal distribution of fission products does not reproduce the long tail observed in the experiment beyond the range of the 591 MeV protons (1.5 Λ). The experimental measurements under considerations are presented in figs 10 and 11. Thus, the assumed sources of evaporation neutrons are not sufficient. Some extra fissions are created by secondary products of p-interactions like pions or neutrons with E_n >20 MeV. The arguments presented by Leroy et al., which exclude pions, are based on the fast decrease of π-production below the 600 MeV incident energy.

A proton induced hadron shower is modelled as follows. The incident proton loses its energy by ionization or by interaction with uranium. The probabilities for the proton induced fission, spallation process or proton elastic scattering are calculated from the energy dependent cross section of [5] for the energy range from 30 to 600 MeV. The 30 MeV proton is assumed to stop. The energy loss by proton in the elastic scattering on uranium is calculated from the coherent elastic formula[17]. For the spallation processes or p-induced fissions only the emission of secondary neutrons is considered. The number of

emitted neutrons is chosen randomly from a Poisson distribution with the average values for neutron multiplicities taken from [38]. Their momenta are sampled from the energy dependent parameterization of the differential cross sections given in [39]. The secondary neutrons can undergo sequential interactions governed by the energy dependent total and differential cross sections from [5] and [39], or are followed in the ONMC model if their energies are below 20MeV. To reproduce the measured spatial distributions of spallation products the multiple scattering of primary protons is not sufficient although it widens the beam radius by ~0.3 cm at 0.6.Λ. The predictions agree well with the experimental data if the width of the proton beam at the entrance point is described by a Gaussian with $\sigma_{xy} \approx 0.8$ cm. This is deduced from the lateral profile of spallation products measured at the depth of 0.6Λ (marked as dots in fig.10).

Longitudinal profiles of spallation, fission and n-capture products are presented in fig.11, while lateral profiles at a depth of 0.6Λ are given in fig.10. Radial distributions in the plane of the U-plates, i.e. perpendicular to the beam direction, for fission and n-captures are given in figs 12-13. The experimental profiles are well reproduced by the calculation.

The longitudinal distribution for fissions beyond 1.5Λ has a long tail caused by secondary fast neutrons (E_n >20 MeV). This confirms that the contribution of the fast neutrons is substantial and that they can carry, besides neutrinos, energy out of heavy material calorimeters. The fact that the longitudinal profiles of fission and spallation products are well reproduced shows that the description of interactions in uranium at several hundred MeV is satisfactory.

The beam spread contributes to the lateral profile of fission products (fig.10), therefore, it makes it less sensitive to the assumption of the ONMC model on the interactions of neutrons of E_n $\leq$20MeV. However the much broader distributions of n-capture products (figs 10-11) are totally due to the model. For the radial distributions (figs 12-13) the assumed beam spread dominates the short distances near the beam, R<3cm, whereas the ONMC model dominates the region R>5 cm leading to the long tails. The distributions are successfully described by the ONMC model.

The distributions might be affected by the leakage of neutrons. Neutrons travel relatively far from their production point. The lateral size of the U-block of 20cm is not sufficient to prevent the leakage of slow neutrons. The measurements are corrected for this leakage. In order to study the amount of leakage, the simulation has been done for an infinitely large U-block and for the experimental setup, i.e. a 20 x 120 x 40 cm^3 U-block. The obtained profiles are consistent within the accuracy of the simulation except for the radial distributions. Some obvious differences in the latter stem from the R>10cm events partially recorded for the limited size U-block, see fig.12 for the plate #41 and the plate #63. Their relative normalization is defined per one primary proton.

Although the spatial distribution are well reproduced, the description of the beam interactions may be too simplified to allow a precise prediction of the number of n-captures

or fissions per incoming proton. Nevertheless, the ratio of the number of n-induced fissions, $E_n \leq 20$ MeV, to the number of n-captures predicted from the ONMC model should agree with the measured values for different compositions of U-plates and scintillator material(Sc). The result is:

	$N^{fission}/N^{n\ capture}$	
	Experimental data	ONMC prediction
U-massive	0.20±0.01	0.20
U(0.3cm)+Sc(0.25cm)	0.14±0.01	0.12
U(0.9cm)+Sc(0.25cm)	0.15±0.02	0.16

Good agreement is observed, although some discrepancies are expected due to the difficulty to correct for the leakage of neutrons in the experiment and the lack of accounting for the ^{235}U-isotope contribution in Monte Carlo.

We conclude that the distributions of fission products and n-capture processes, mainly dominated by the low energy neutron processes, are well reproduced. The ONMC code is a reliable and satisfactory description of neutron-uranium nuclear processes.

6. Neutron Detection

The main interest in neutrons for calorimetry comes from the possibility to tune their contribution to the signal in such a way that an equal response is obtained for electrons and hadrons and thus achieve an optimum energy resolution [3-8,31,33,34] in uranium(lead)-scintillator calorimeters.

The precision of the energy measurement in a compensating calorimeter is partially defined by the event-to-event fluctuations coming from the large variety of possible nuclear reactions and from nuclear binding energy losses. Efficient neutron detection reduces considerably the effect of these fluctuations since the number of emitted neutrons is strongly correlated with the binding energy loss. To achieve the best resolution it is necessary to understand in detail the fundamental processes of hadronic shower detection as well as the effects of inactive material required for structural reasons and the effects of the finite size of the detectors and the finite signal integration time.

In this section we shall try to express the contribution of the neutron component to the calorimeter signal and to the calorimeter resolution in the form of a single neutron signal, that is, we want to calculate the one-neutron signal, $< signal >_{1n}$, and the one-neutron resolution, $\sigma_{1n}^{signal} / < signal >_{1n}$. On the basis of the one-neutron signal we shall then examine effects related to the physics of neutron production and neutron transport, and to the details of the calorimeter design. Finally, a few comments on the full hadronic shower are given.

As discussed in section 2 the neutron component produced in a hadronic interaction is determined by the amount of nuclear excitation energy which is left after the emission of

the internuclear cascade particles. The fraction of the deexcitation energy converted into neutrons varies from interaction to interaction. It depends strongly on the energy and the type of the interacting hadron, on the number of cascade particles emitted and on the type of secondary particles. It produces a kind of statistical fluctuations constrained by energy and momentum conservation. The dispersion of the neutron component signal can be assumed to be given by the dispersion of the multiplicity of evaporation neutrons and by the neutron detection. The latter, i.e. the one neutron resolution, has contributions from the natural spread of the evaporation neutron spectrum, $\sigma_{Maxwell}/\bar{E}_n$=0.8, plus contributions related to the neutron cascade development and to the efficiency of the readout material.

For a better understanding of the problem it is instructive to compare the signal generated by one neutron to the signal created by a group of neutrons in a uranium compensating calorimeter, fig.14 (see also fig.6). The one-neutron signal is subject to large non-Gaussian fluctuations. The distribution, however, approaches a Gaussian distribution with increasing number of neutrons, N, contributing to the signal. To illustrate this, the fourth moment of the signal distribution minus three, called kurtosis, is presented in fig.15 as a function of N for the uranium compensating calorimeter, gas-uranium ones and lead compensating calorimeter. In a 10 GeV hadronic shower the number of evaporation neutrons in heavy materials is above 200 [2,7]. This number is large enough to justify the statistical averaging of the signal, proposed above. However locally, with the mean number of neutrons per interaction of around 5-15 [12,38], the averaging needs a cautious treatment at least due to the lack of "symmetry" in the signal distribution.

In the simulation a point-like source of neutrons is situated at the center of a calorimeter but spread homogeneously along the thickness of the absorber plate to avoid any local effects. The calorimeter has an infinite depth, 200 x 200 cm^2 lateral size interspersed with 0.26 scintillator plates and uranium plates of variable thickness, if not stated otherwise.

The crucial role of the so-called e/h-ratio for the energy resolution and the way to "tune" the hadron response by varying the ratio of uranium plate thickness to scintillator thickness [7] is a well recognized fact. Our attention is concentrated on the dependence of the one-neutron response on the ratio of the thicknesses of the absorber plate and the scintillator, fig.16. It is also of interest to study effects caused by (i) the different mean energy of evaporation neutrons for lead (see sect.2) and by (ii) gaseous readout.

The efficiency of the neutron signal collection, called the sampling fraction α_n, is defined here as the fraction of the kinetic energy of the emitted neutron observed as signal after taking into account the light saturation effects, $\alpha_n = C \cdot \frac{<signal>}{\bar{E}_n}$; in the studies, the efficiency C of the signal conversion into the detected photons is assumed to be equal to 1. In fig.16a we show the sampling fractions for neutrons as a function of the ratio of the absorber to scintillator plate thicknesses. For the ZEUS calorimeter, where d_{absr}/d_{Sc}=1.27, we see that the neutron sampling fraction is around 10.8%. For comparison, the charge

sampling fraction for a minimum ionizing particle is 7%. As discussed before the slow change of efficiency with the amount of absorber is due to the important contribution of the first n–p scatter to the energy transfer. The efficiency is similar for lead and uranium. It increases slightly with decreasing energy of the evaporation neutrons. This is due to changes of the amount of the energy loss in inelastic scattering processes.

Fig.16b shows the spread of the one neutron signal which increases as a function of d_{absr}/d_{Sc}. For the thick uranium layers the resolution of neutrons becomes worse due to the increasing importance of fluctuation introduced by fission processes. The tendency is visible by looking at uranium calorimeters with gaseous readout: the fluctuations are huge due to fission and undetected neutrons, the signal is tiny. From the numbers given in Table 3 and the discussion presented in section 4.3 one expects that evaporation neutrons are a significant source of fluctuations in hadronic showers.

In contrast to uranium sampling calorimeters, the fluctuations of neutron detection in lead (fig.16b) are less pronounced. However, the essential differences in the neutron component produced by a hadron shower in lead and in uranium originate from the difference in yield of evaporation neutrons (see sect.2). Neutrons are abundantly produced in uranium by high-energy fission induced by hadrons in the energy range of several hundreds of MeV.

The work presented here, was motivated by a series of experimental investigations performed by the ZEUS collaboration[33,34]. One of the prototype calorimeters consisted of 4 modules, each of the 60 x 60 cm^2 lateral size and a depth of about 1.5 interaction length of absorber interspersed with thin layers of air and/or iron, in addition to the scintillator and absorber. In this set-up, the neutron detection efficiency is limited by:

- the transverse size of the calorimeter;
- the leakage through the front wall of the calorimeter and effects of inactive material inside the calorimeter needed for construction;
- the size of a slot between consecutive modules;
- the air gaps between absorber and scintillator.

In our simulation a uranium sampling calorimeter of 60 x 60 cm^2 lateral size is taken with 0.33 cm thick absorber plates and 0.26 cm scintillator plates. The neutron leakage out of a calorimeter affects the efficiency of their detection. It has already been shown that gaseous readout causes a leakage due to the small stopping power of gases. A similar leakage is expected if there is a gap after each sequential layer (fig.17), which affects the full neutron component. One can see that a sequential gap of 0.2cm thickness leads to the loss of 8% of the signal, whereas for a 0.5cm gap the loss is larger than 20%. The bad resolution measured for the gas-uranium sampling calorimeters of [32] is not only due to the small

sampling fraction of gas readout but also to the gaps which are, at least, 0.5 cm wide. The same effect is observed around any kind of module boundary like the front, side walls or its end (fig.18). It affects a region of $R_{XY}^{signal}/\sqrt{2}$ cm. Another detector put next to the module under investigation (here, at the distance of 10 cm) diminishes but does not cancel this leakage.

In summary, the neutron component is very sensitive to the mechanical details of the calorimeter in a quite large area. This is in contrast to the charged component of hadronic showers, which is influenced only by materials placed within a few centimeters ($\sim$ 3cm) around the incident beam; the neutron component is affected by materials within tens of centimeters around it.

The neutron contribution to the hadron shower detection in a uranium calorimeter has been discussed in [3]. Using the one-neutron signal, the authors studied the resolution of an infinitely large uranium scintillator calorimeter. A energy resolution of $0.30/\sqrt{E[GeV]}$ has been obtained for a calorimeter consisting of 0.3 cm thick U-plates and 0.25 cm scintillator plates. A similar analysis, repeated here for the above infinitely long calorimeter with a lateral size of 60 x 60 cm^2 interspersed with 0.5 cm thick gaps between each sequential plates, shows a degradation of the resolution to $0.37/\sqrt{E}$ for 5 GeV pions. The calorimeter signal decreases by about 15%. The leakage of neutrons affects strongly the calorimeter signal and the energy resolution.

7. Conclusions

Based on experimental as well as on theoretical studies, the crucial role of neutron detection for hadron calorimetry is now generally accepted. To investigate the neutron component of a hadron shower and the neutron contribution to the calorimeter signal, the detailed **"One Neutron Monte Carlo"** programme has been developed to simulate the behaviour of neutrons with energies below 20 MeV. The code allows a fast and easy estimation of contributions of various effects and their consequences. It allows to determine which processes are the dominant ones.

The ONMC has been compared in detail with the available experimental information. It agrees quite well with them. Even when agreement is not totally perfect it can guide the user to make correct decisions.

The code can be used for other purposes than discussed here, e.g. to simulate photoneutrons and their consequences in the electromagnetic shower development or to get a parameterization of the neutron cascade for any hadron shower model.

The calculations presented here indicate that the efficiency for detection of an evaporation neutron in lead and in uranium is comparable. The signal from neutrons in calorimeters with gaseous readout exhibits large fluctuations.

The neutron contribution to the calorimeter resolution is very sensitive to the technical

details of the detector construction such as lateral size, depth, gaps and inactive material. Any effect which leads to extra leakage, neutron absorption, or a reduction of the neutron detection worsen the resolution. It has been found that sequential air gaps between sampling layers deteriorate the resolution significantly.

Acknowledgments

The author wishes to thank DESY directorate for the financial support and her colleagues at DESY for their hospitality, help and understanding. The author is indebted to B.Anders, R.Klanner, D.Notz, G.Wolf and J.Zakrzewski for their continuous interest, advice and encouragement. This paper benefits considerably from their suggestions. The work started in the collaboration with H.Kowalski. Special thanks to him for directing my interest to the problem.

Table 1.

Uranium calorimeter 200 x 200 x 1000 cm^3

per EVAPORATION neutron $\bar{E}_n$=3.55MeV				
		Pure U	U(0.33)+Sc(0.26)	U(1.0)+Sc(0.26)
	Λ_{coll}^{eff}[cm]	2.7	3.3	3.0
	Λ_{int}^{eff}[cm]	6.2	8.3	7.4
Number of interactions				
U	elastic	~80	12	26
	inelastic	6.7	1.2	2.4
	(n,2n)	0.06	0.04	0.05
	(n,3n)	0.003	0.002	0.003
	fission	0.36	0.17	0.26
	n-capture	1.77	1.38	1.6
H_2	elastic		10	8
C	elastic		3.2	2.5
	abs+inel		0.01	0.007
Amount of energy deposited [MeV]				
U	elastic	0.15	0.02	0.04
	inelastic	3.3	1.5	2.3
	(n,2n)	0.5	0.3	0.4
	(n,3n)	0.03	0.03	0.03
	fission			
	n-capture	0.45	0.07	0.14
H_2	elastic		1.6	1.0
C	elastic		0.26	0.16
	abs+inel		0.08	0.04
Spatial spread [cm]				
	$R_{XY}^{fission}$	17	17	17
	$R_{XY}^{n\ capt.}$	32	20	23
Signal				
	Signal[MeV]		0.39	0.22
	$t^{signal}[ns]$		17	30
	$R_{XY}^{signal}[cm]$		18	18

Table 2.

Lead calorimeter 200 x 200 x 1000 cm^3

per EVAPORATION neutron $\bar{E}_n$=3.55MeV				
		Pure Pb	Pb(0.33)+Sc(0.26)	Pb(1.0)+Sc(0.26)
	Λ_{coll}^{eff}[cm]	4.7	4.7	4.7
	Λ_{int}^{eff}[cm]	20.7	19.3	16.6
Number of interactions				
Pb	elastic	~600	9	25
	inelastic	1.2	0.3	0.5
	(n,2n)	0.03	0.02	0.03
	(n,3n)	<0.0001	0.001	0.003
	n-capture	0.3	~0.3	~0.6
H_2	elastic		15.3	14.9
	n-capture		~0.7	~0.4
C	elastic		4.1	3.6
	abs+inel		0.02	0.01
	leakage	0.7	0.	0.0001
Amount of energy deposited [MeV]				
Pb	elastic	0.45	0.02	0.04
	inelastic	2.5	1.1	1.6
	(n,2n)	0.3	0.2	0.2
	(n,3n)	0	0.02	0.04
	n-capture	<0.0001	0.03	0.06
H_2	elastic		1.74	1.28
C	elastic		0.3	0.2
	abs+inel		0.1	0.04
Spatial spread [cm]				
	$R_{XY}^{n\ capt.}$	~120	~30	~40
Signal				
	Signal[MeV]		0.45	0.29
	$t^{signal}[ns]$		21	45
	$R_{XY}^{signal}[cm]$		24	29

Table 3.

Gas sampling calorimeter 200 x 200 x 1000cm^3
0.33 cm U-plates; 0.66 cm gas chambers

per EVAPORATION neutron $\bar{E}_n$=3.55MeV			
		C_4H_{10}	CH_4
	Λ_{coll}^{eff}[cm]	8.2	8.0
	Λ_{int}^{eff}[cm]	18.1	19.1
Number of interactions			
U	elastic	~68	~71
	inelastic	5.8	6.1
	fission	0.35	0.36
	n-capture	1.56	1.57
H_2	elastic	0.79	0.33
C	elastic	0.13	0.03
	leakage	0.17	0.18
Amount of energy deposited [MeV]			
U	inelastic	3.2	3.2
H_2	elastic	0.11	0.048
		(0.23)*	(0.17)*
C	elastic	0.006	0.002
	leakage	0.0001	0.0001
Spatial spread [cm]			
	$R_{XY}^{fission}$	~51	~51
	$R_{XY}^{n\ capt.}$	~80	~80
Signal			
	Signal [MeV]	0.013	0.005
		(0.031)*	(0.021)*
	R_{XY}^{signal} [cm]	~72	~73

*/per detected neutron, i.e. if no contribution to signal, neutron is excluded.

Figures Captures

Fig.1 The Maxwell spectra of evaporation neutrons for mean kinetic energies of 2 MeV and 3.55 MeV without relative normalization.

Fig.2 Cross sections for n-^{238}U interactions as functions of the neutron kinetic energy.

Fig.3 Cross sections for n-^{nat}Pb interactions as functions of the neutron kinetic energy.

Fig.4 Cross sections for n-^{12}C interactions and n–p elastic scattering as functions of the neutron kinetic energy.

Fig.5 Neutron signal as a function of the energy of monoenergetic neutrons in compensating calorimeters: the full line is for uranium-scintillator, the dashed line is for lead scintillator; the shaded area corresponds to the accuracy of modelling neutron interactions on uranium.

Fig.6 Spectrum of neutron signals E per evaporation neutron in calorimeters with 0.33 cm thick U-plates and (i) 0.26 cm thick scintillator and (ii) 0.66cm isobutane readout.

Fig.7 Lateral profile of neutron signal in uranium-scintillator compensating calorimeters with the neutron source situated at X=0. The equivalent profile for isobutane-uranium composition is included.

Fig.8 Neutron time signal for U+Sc calorimeters: (i) 0.33cm U + 0.26cm Sc and (ii) 1.0cm U + 0.26cm Sc.

Fig.9 Neutron spatial spread, R_{XY}, defined as the radius with 90% containment of a process as a function of thicknesses of absorber plates (with scintillator 0.26 cm) for signal, fissions and neutron captures in uranium and lead. For a visual comparison, the neutron spread of fission and of neutron captures in massive U-block is included.

Fig.10 The measured lateral profiles of spallation products (circles), fission products (squares) and n-capture products (triangles) for 591 MeV protons at a depth of 0.6Λ in a U-block [8] are compared with the ONMC prediction (histograms).

Fig.11 Longitudinal distribution of spallation, fission and neutron capture products from 591 MeV protons. The ONMC prediction (histograms) is compared to the measurements [8] (dots); the measured concentrations of fission products ^{103}Ru are presented as circles while ^{131}I — in a form of two lines each marking edges of the experimental errors.

Fig.12 Radial distribution, R, of neutron capture products from 591 MeV protons for an infinitely large block of uranium in the U-plates (#02, #20, #41, #63, #83) and for 20 x 120 x 40 cm^3 block in the U-plates (#41, #63). The ONMC prediction (histograms) is compared to the measurements [8] (dots) which are normalized to the simulation in the infinite U-block.

Fig.13 As in fig.12 but for the fission products;

Fig.14 The signal E of a single neutron and the signal created by a group of N-neutrons (in arbitrary units) for N=10 and 100.

Fig.15 The kurtosis of neutron signal distributions in a uranium compensating calorimeter(full line), the lead compensating calorimeter(dotted line) and the gas-uranium calorimeters (methane – dashed-dotted line, isobutane – dashed line) as a function of number of neutrons,N, creating the signal. It is expected to be zero for a Gaussian distribution.

Fig.16 The neutron sampling fraction α_n (a), and the one neutron resolution, $\sigma_{1n}^{signal}/ < signal >_{1n}$, (b), as a function of the ratio of thicknesses of absorber and scintillator, d_{absr}/d_{Sc}, per evaporation neutron for uranium and lead calorimeters. For lead the calculations are done for mean neutron energies of 3.55 MeV and 2 MeV(see sect.2). A scintillator thickness of 0.26 cm is taken for all the calculations. For a visual comparison the results of gas-uranium calorimeters are added and placed at d_{absr}/d_{Sc}=(0.33cm/0.66cm)=0.5 as squares for isobutane and as triangles for methane. It should be scaled as $(d_U/\Lambda_U)/(d_{readout}/\Lambda_{readout})$, but it leads to an unclear graph.

Fig.17 The fraction of the detected neutron signal S (dashed line) and the resolution (full line) as a function of the size of gaps inside the uranium compensating calorimeter.

Fig.18 Studies of the effects of inhomogeneity in calorimeter geometry (a front wall, dead material, limited transversal size of a calorimeter); this figure presents the neutron sampling fraction (a) and neutron resolution (b) calculated as a function of the distance X of the evaporation neutron source from inhomogeneous point for the uranium compensating calorimeter. The dashed line — if another detector is nearby, here at a distance of 10 cm.

References

1. ZEUS status report, 1988.

2. For a discussion of experimental data from multi-GeV interactions, see B.D.Wilkins, E.P.Steinberg, S.B.Kaufman, Phys. Rev, C19(1979)856 and references there; the hundreds-MeV-experimental data are summarized by F.S.Alsmiller, R.G.Alsmiller, T.A.Gabriel, R.A.Lille, J.Barish, Nuclear Science and Engineering, 79(1981)147.

3. H.Kowalski, H.-J.Moehring, T.Tymieniecka, DESY 87-170.

4. F.Barreiro, G.Cases, P.Cloth, K.Dierks, G.Drews, J.Engelen, D.Filges, M.A.Garcia, R.Klanner, U.Kötz, J.Krüger, G.Levman, J.Martin, H.J.Möhring, F.Selonke, G.Sterzenbach, J.Straver, H.Tiecke, T.Tymieniecka, DESY 89-171.

5. P.Cloth, D.Filges, R.D.Neef, G.Sterzenbach, Ch.Reul, T.W.Amstrong, B.L.Colborn, B.Anders, H.Brückmann, Juel-2203, 1988; B.Anders, P.Cloth, D.Filges, Ch.Reul, G.Sterzenbach, Nucl. Inst. and Meth., A277(1989)56.

6. C.Leroy, Y.Sirois, R.Wigmans, Nucl. Inst. and Meth., A252(1986)4.

7. H.Brückmann, B.Anders, U.Behrens, P.Cloth, D.Filges, DESY 87-064; H.Brückmann, U.Behrens, B.Anders, DESY 86-155.

8. R.Wigmans, Nucl. Inst. and Meth., A259(1987)61.

9. FLUKA86 user's guide, P.A.Aarnio, A.Fasso, H.-J.Moehring, J.Ranft, G.R.Stevenson, CERN, TIS-RP/168(1986) and TIS-RP/190(1987).

10. Particle Properties Data Booklet, from "review of Particle Properties", Physics Letters , B170(1986).

11. T.Nakamura, Nucl. Inst. and Meth., A240(1985)207.

12. A summary of references with a compact review of studies for hundreds-MeV interactions is done by T.Nakamura, Y.Uwamino, K.Sato, Y.Furuta, S.Tanaka, S.Ban, H.Hirayama, T.Kosako, K.Kawachi, Y.Nishihara, Atomic Data and Nuclear Data Tables, 32(1985)471.

13. S.Fredriksson, G.Eilam, G.Berlod, Physics Reports, 144(1987)188.

14. D.E.Groom, Radiation Levels in the SSC Interaction Region, SSC-SR-1033, 1988.

15. S.S.Dietrich, B.L.Berman, Atomic Data and Nuclear Data Tables, 38(1988)199; B.Forkmann, R.Petersson, IAEA, Technical Report Series, No 273, Handbook on Nuclear Activation Data, Vienna,1987.

16. V.M.Gorbachev, Y.S.Zamyatin, A.A.Lbov, Nuclear Interactions in Heavy Elements, Pergamon Press (1980) and references there.

17. J.Ranft, J.T.Routti, Particle Accelerators, 4(1972)101.

18. E.Barnard, A.T.G.Ferguson, W.R.McMurray, I.J.van Heerden, Nucl. Phys., 71 (1965)228.

19. G.Haouat, J.Lachkar, C.Lagrange, J.Jary, J.Sigaud, Y.Patin, Nuclear Science and Engineering, 81(1982) 491.

20. L.E.Beghian, G.H.Kegel, T.V.Marcella, B.K.Barnes, G.P.Couchell, J.J.Egan, A.Mittler, D.J.Pullen, W.A.Schier, Nuclear Science and Engineering, 69(1979) 191.

21. G. de Saussure, A.B. Smith, Nuclear Data for Science and Technology, ed. K.H.Bockhoff (1983) and references therein.

22. A.B. Smith, Proceedings of Antwerp Conference, (1983) and references there.

23. R.J.Howerton, Nuclear Science and Engineering, 62(1977) 438.

24. P.Plischke, R.Langkau, W.Scobel, R.Wien, Nukleonika, 27(1982)285.

25. E.Sheldon, Nuclear Data for Science and Technology, ed. K.H.Bockhoff (1983); E.Sheldon et al., Journal of Physics G, Nucl. Phys. 12(1986)443.

26. P.E.Hodgson, A.M.Kobos, Nuclear Science and Engineering, 89(1982) 111.

27. M.Craner, M.Segev, S. Yiftah, Nuclear Science and Engineering, 59(1976) 395; see also, H.Kamus, A.Ackermann, W.Scobel, J.Phys.G:Nucl.Phys., 5(1979)715.

28. J.H.Towle, W.B.Gilboy, Nucl. Phys., 44(1963)256; L.Cranberg, T.A.Oliphant, J.Levin, C.D.Zafiratos, Phys. Rev., 159(1967)969.

29. C.Y.Fu, F.G.Perey, Atomic Data and Nuclear Data Tables, 16(1975)409 and references therein.

30. J.A.Janni, Atomic Data and Nuclear Data Tables, 27(1982)147.

31. E.Bernardi, G.Drews, M.A.Garcia, R.Klanner, U.Kötz, G.Levman, M.Lomperski, D.Lüke, E.Ros, F.Selonke, H.Tiecke, M.Tsirou, W.Vogel, Nucl. Inst. and Meth., A262(1987)229.

32. Y.Galaktionov, A.Gordeev, Y.Gorodkov, Y.Kamyshkov, A.Klimentov, A.Kunin, V.Koutsenko, A.Malinin, V.Morgunov, V.Plyaskin, V.Pojidaev, A.Savin, V.Shevchenko, E.Shumilov, V.Shoutko, E.Tarkovsky, V.Tchudakov, S.C.C.Ting, T.Azemoon, R.C.Ball, I.D.Leedom, M.J.Longo, Nucl. Inst. and Meth., A251(1986)258.

33. a recent review of the ZEUS test results, e.g. R.Klanner, Nucl. Inst. and Meth., A265(1988)200.

34. G.D'Agostini, A.Bamberger, F.Barreiro, E.Bernardi, K.Dierks, G.Drews, J.Engelen, M.Garcia, R.Klanner, U.Kötz, J.Krüger, G.Levman, D.Lüke, J.Martin, E.Ros, F.Selonke, R.van der Stad, J.Straver and H.Tiecke, Nucl. Inst. and Meth., A274(1989)134.

35. J.E.Brau, T.Gabriel, ORNL/TM-10903(1989); J.E.Brau, T.Gabriel, Nucl. Inst. and Meth., A279(1989)40; HETC–The High Energy Transport Code, T.A.Gabriel, ORNL/TM-9727(1985).

36. M.B.Emmet, ORNL-4972/R1(1983).

37. B.Anders, R.Beckmann, U.Brandenburg, H.Brückmann, Jahresbericht, I. Institut für Experimentalphysik 1984/85, Hamburg University; see also [7] and references given therein.

38. T.W.Amstrong, P.Cloth, D.Filges, R.D.Neef, Nucl. Inst. and Meth., 222(1984)540 and references therein.

39. K.Tsukada, Y.Nakahara, Atomkernenergie, Kerntechnik, 44(1984)186.

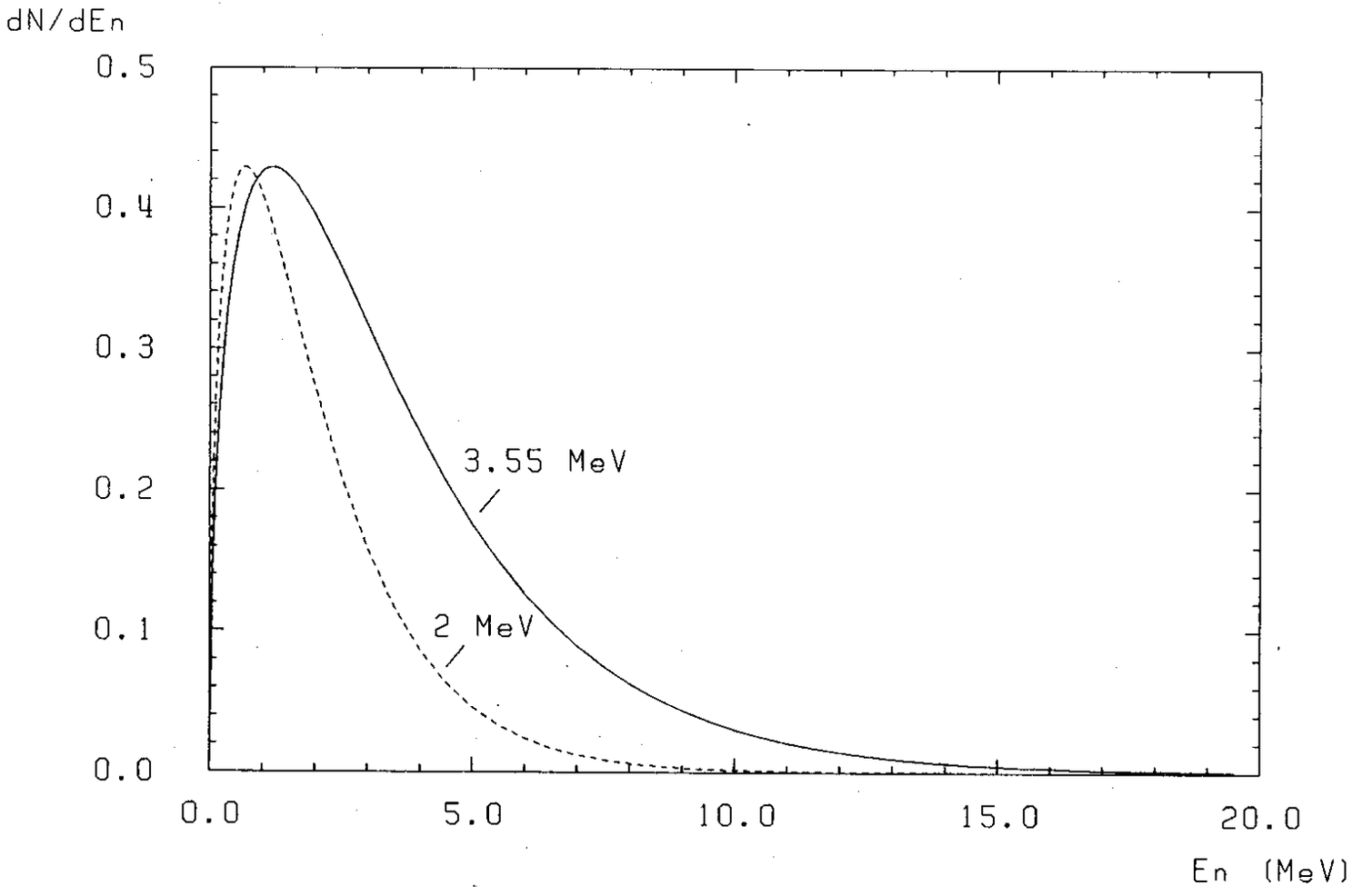

Fig.1 The Maxwell spectra of evaporation neutrons for mean kinetic energies of 2 MeV and 3.55 MeV without relative normalization.

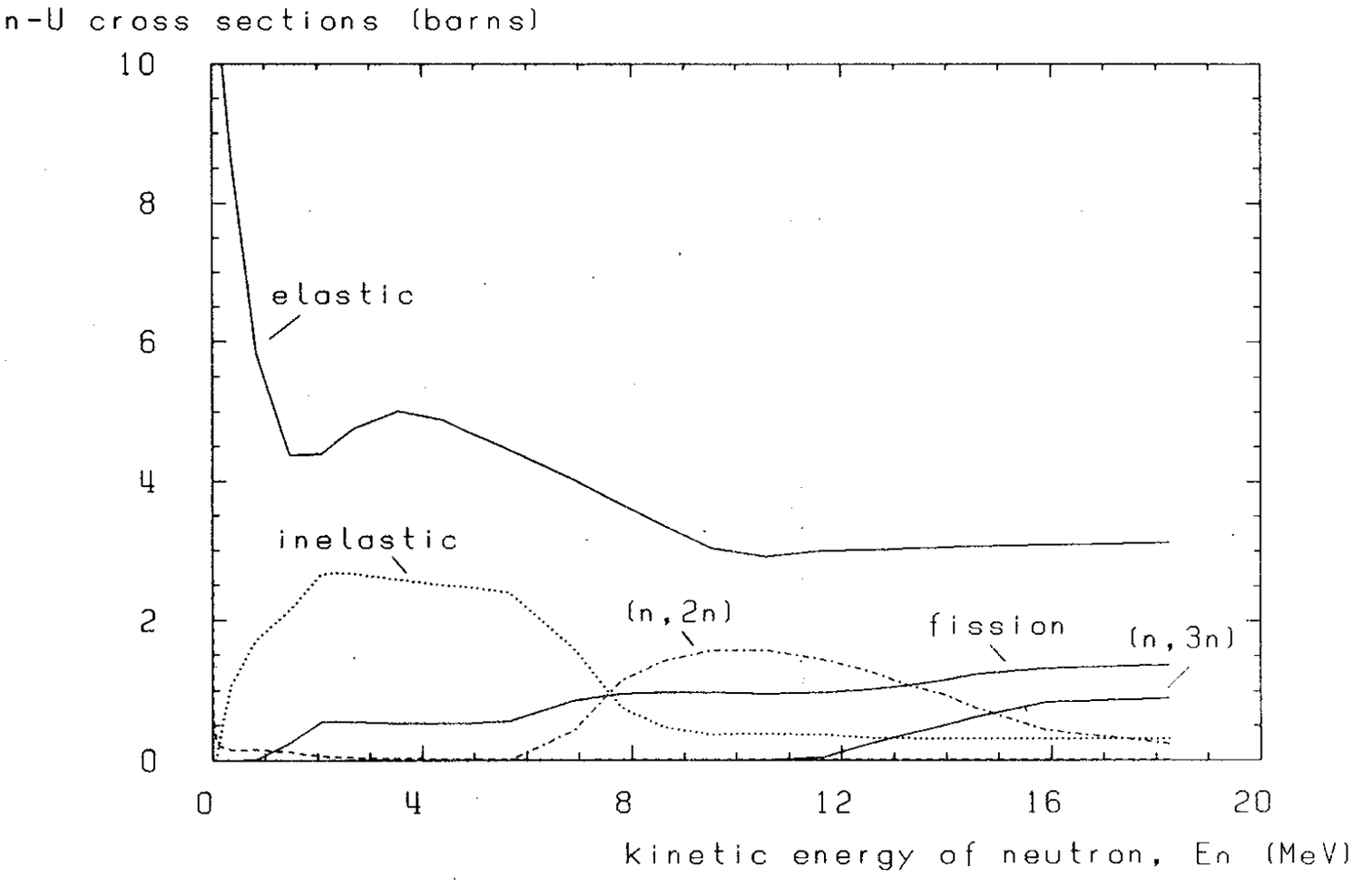

Fig.2 Cross sections for n-^{238}U interactions as functions of the neutron kinetic energy.

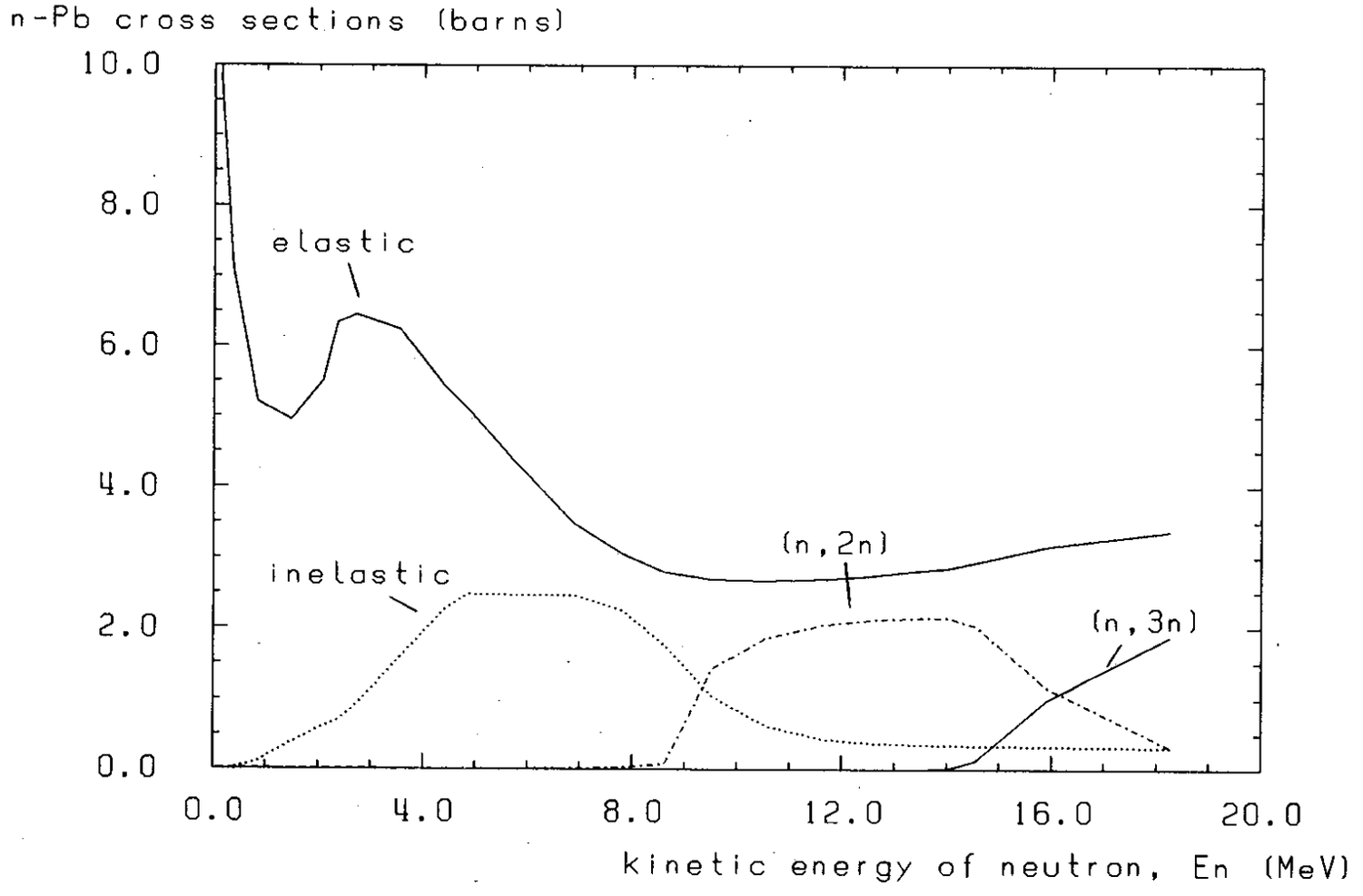

Fig.3 Cross sections for n-^{nat}Pb interactions as functions of the neutron kinetic energy.

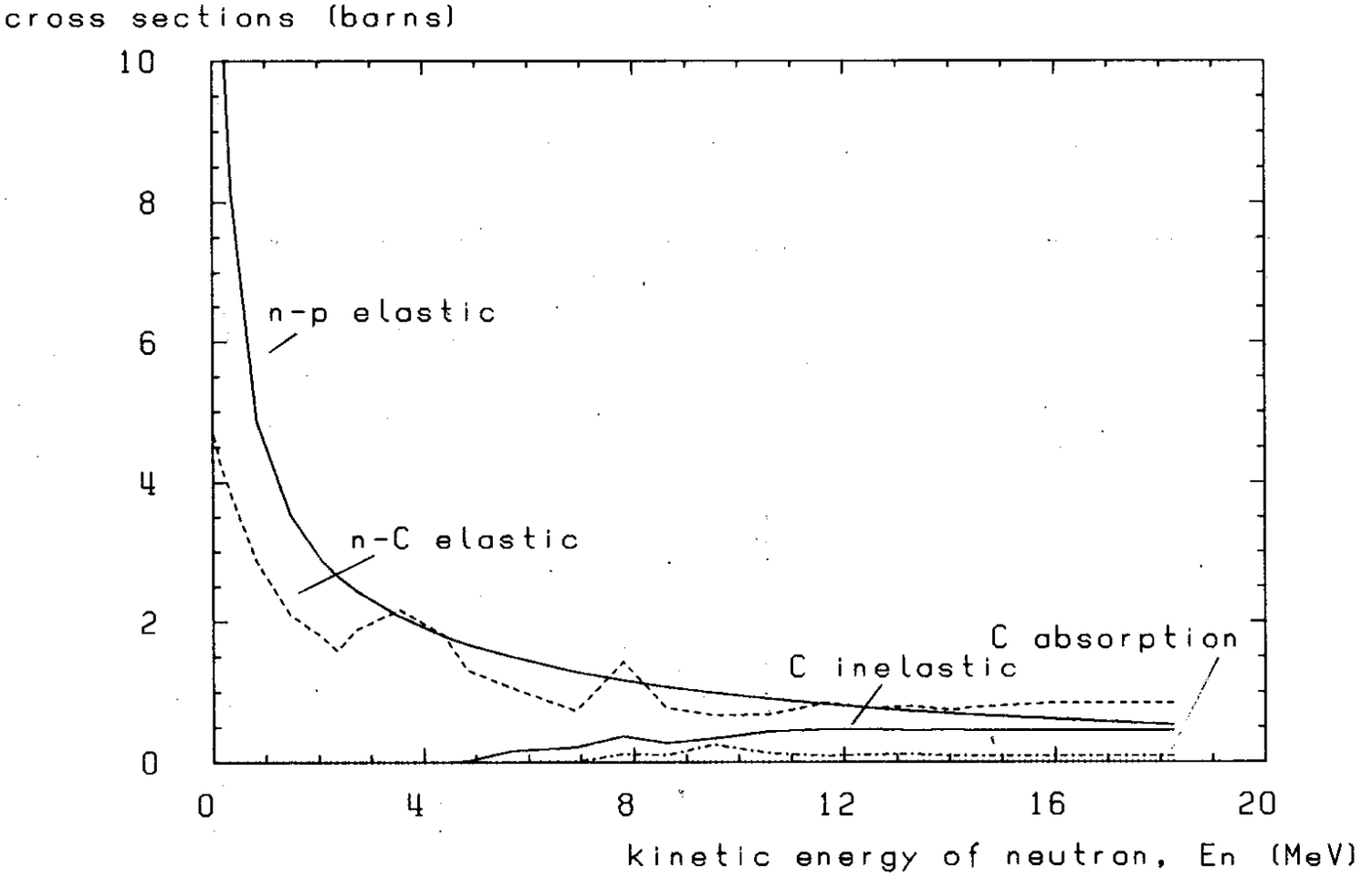

Fig.4 Cross sections for n-^{12}C interactions and n–p elastic scattering as functions of the neutron kinetic energy.

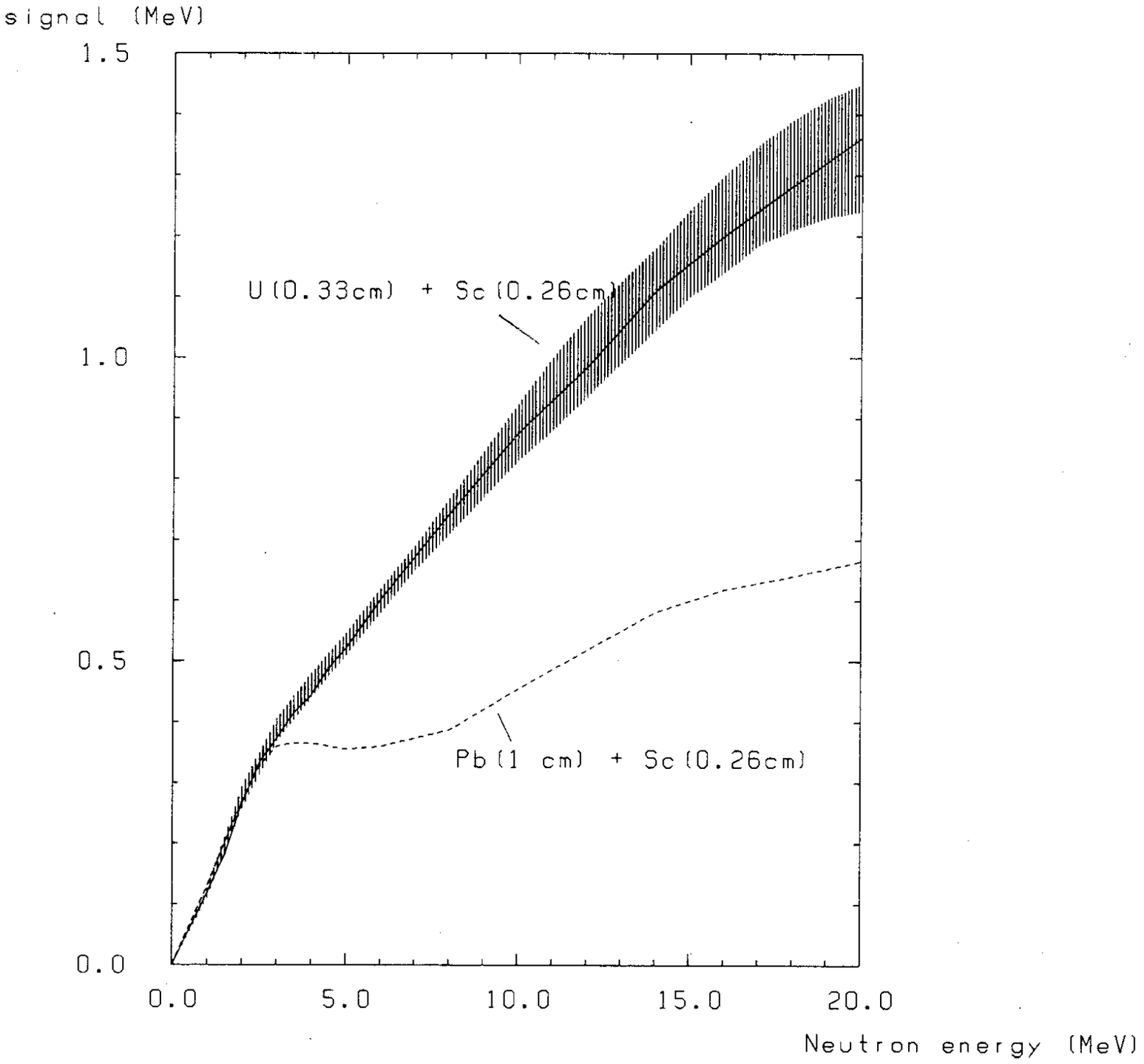

Fig.5 Neutron signal as a function of the energy of monoenergetic neutrons in compensating calorimeters: the full line is for uranium-scintillator, the dashed line is for lead scintillator; the shaded area corresponds to the accuracy of modelling neutron interactions on uranium.

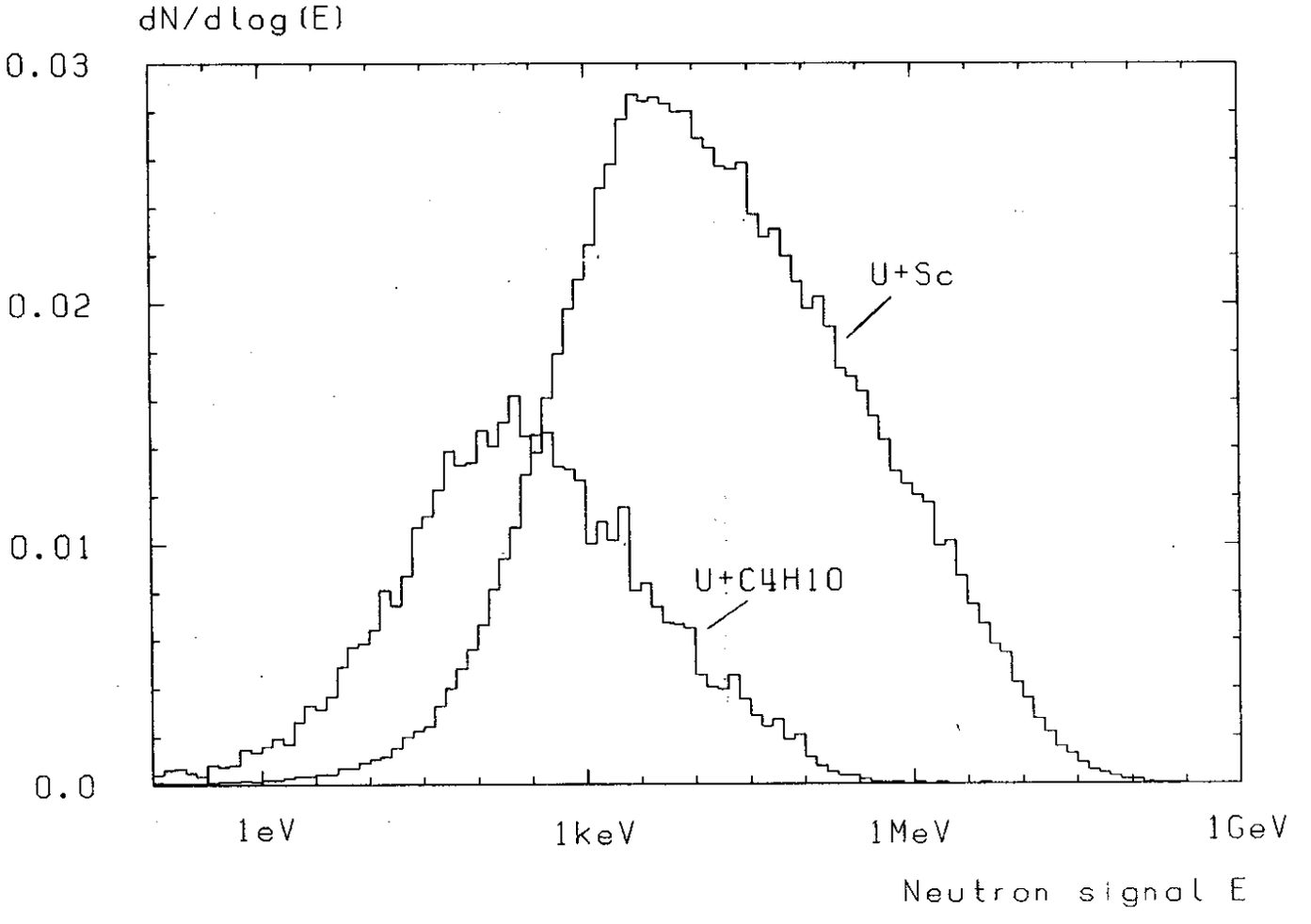

Fig.6 Spectrum of neutron signals E per evaporation neutron in calorimeters with 0.33 cm thick U-plates and (i) 0.26 cm thick scintillator and (ii) 0.66cm isobutane read-out.

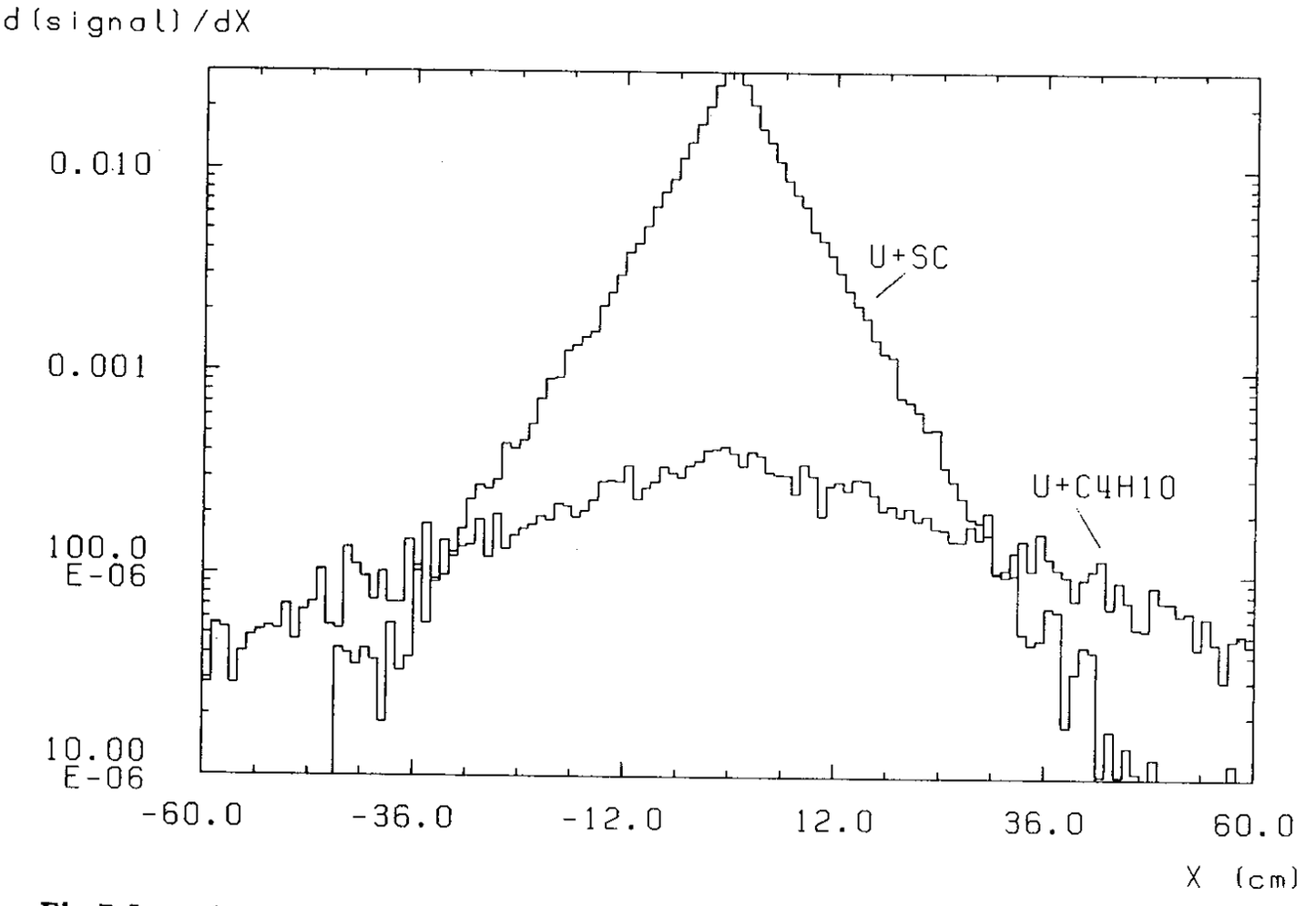

Fig.7 Lateral profile of neutron signal in uranium-scintillator compensating calorimeters with the neutron source situated at X=0. The equivalent profile for isobutane-uranium composition is included.

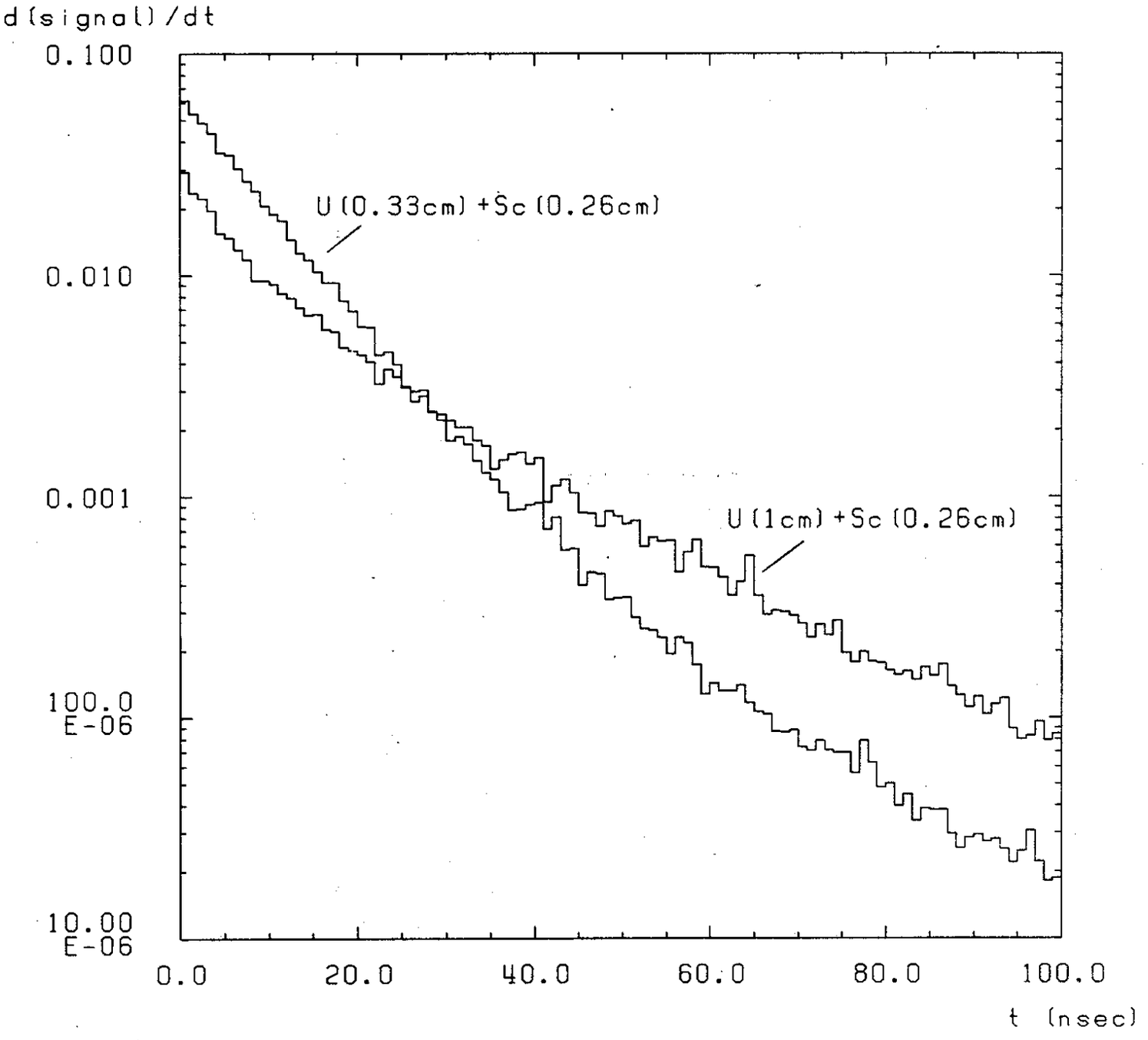

Fig.8 Neutron time signal for U+Sc calorimeters: (i) 0.33cm U + 0.26cm Sc and (ii) 1.0cm U + 0.26cm Sc.

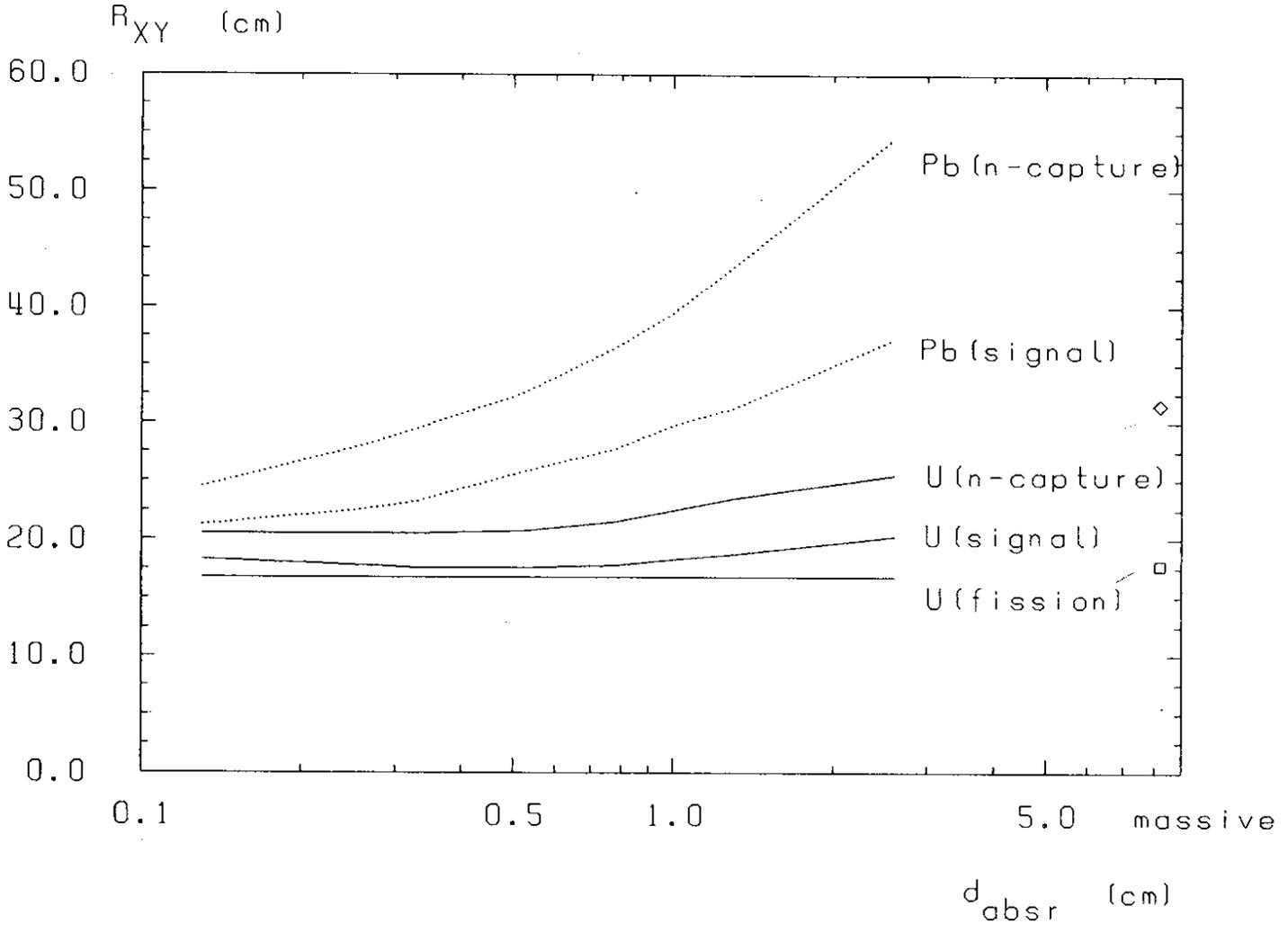

Fig.9 Neutron spatial spread, R_{XY}, defined as the radius with 90% containment of a process as a function of thicknesses of absorber plates (with scintillator 0.26 cm) for signal, fissions and neutron captures in uranium and lead. For a visual comparison, the neutron spread of fission and of neutron captures in massive U-block is included.

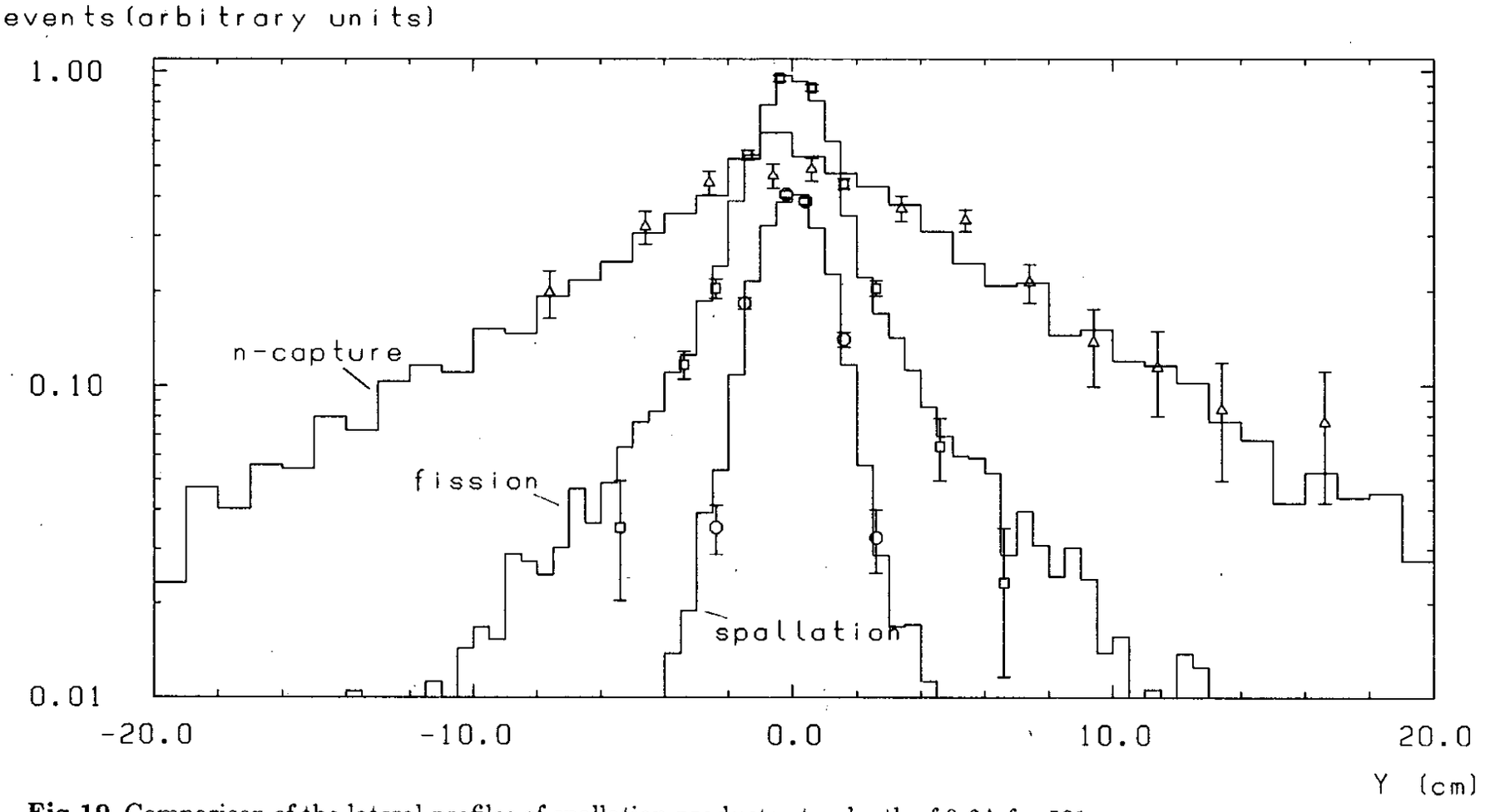

Fig.10 Comparison of the lateral profiles of spallation products at a depth of 0.6Λ for 591 MeV protons simulated with the beam spread in space (see text) to experimental values (dots) taken from ref. 8.

Lateral profiles of fission and neutron capture products from 591 MeV protons at a depth of 0.6Λ (no relative normalization); the simulations (histograms) are compared with the experimental values (squares for fissions, triangles for n-captures) taken from ref. 8.

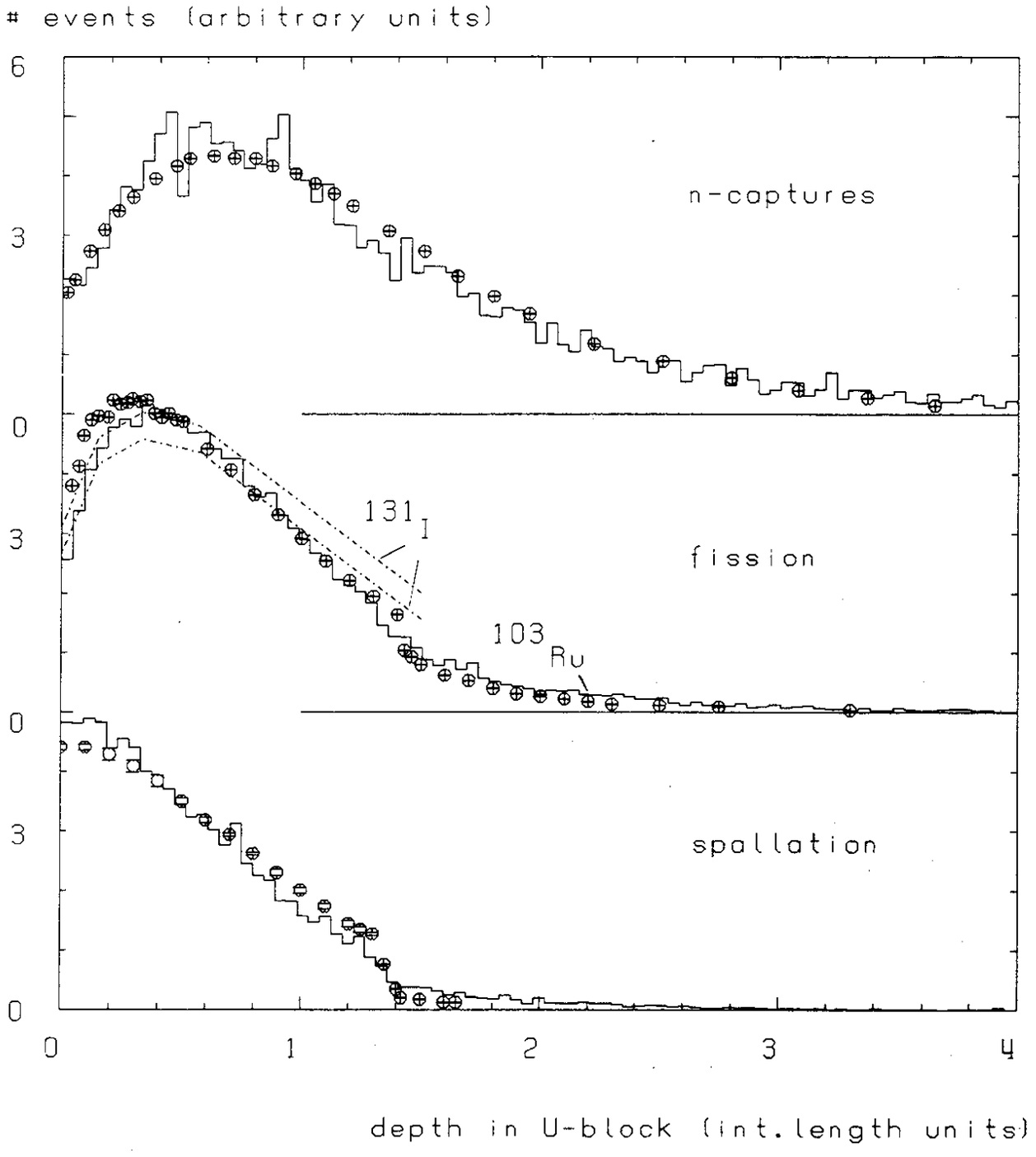

Fig.11 Longitudinal distribution of spallation, fission and neutron capture products from 591 MeV protons. The simulations (histograms) are compared to the measured concentrations taken from ref. 8 and presented as dots for spallations; the measured concentrations are presented as points for ^{103}Ru and in a form of two lines each marking edges of the experimental errors for ^{131}I.

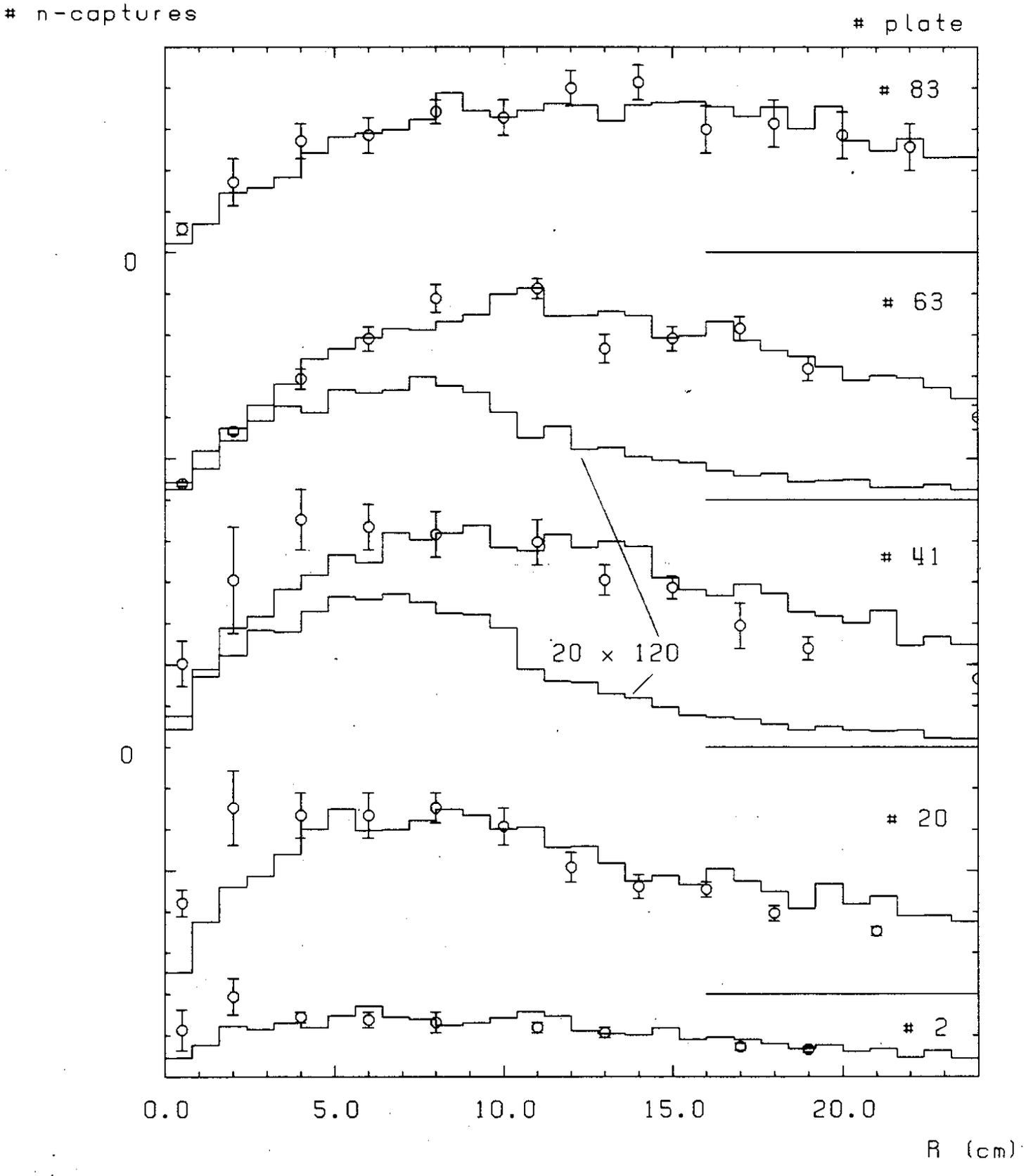

Fig.12 Radial distribution, R, of neutron capture products from 591 MeV protons for an infinitely large block of uranium in the U-plates (#02, #20, #41, #63, #83) and 20 x 120 cm^2 block for the U-plates (#41, #63). The simulations (histograms) are compared to the measured concentrations taken from ref. 8 and presented as dots normalized to the simulation in the infinite U-block.

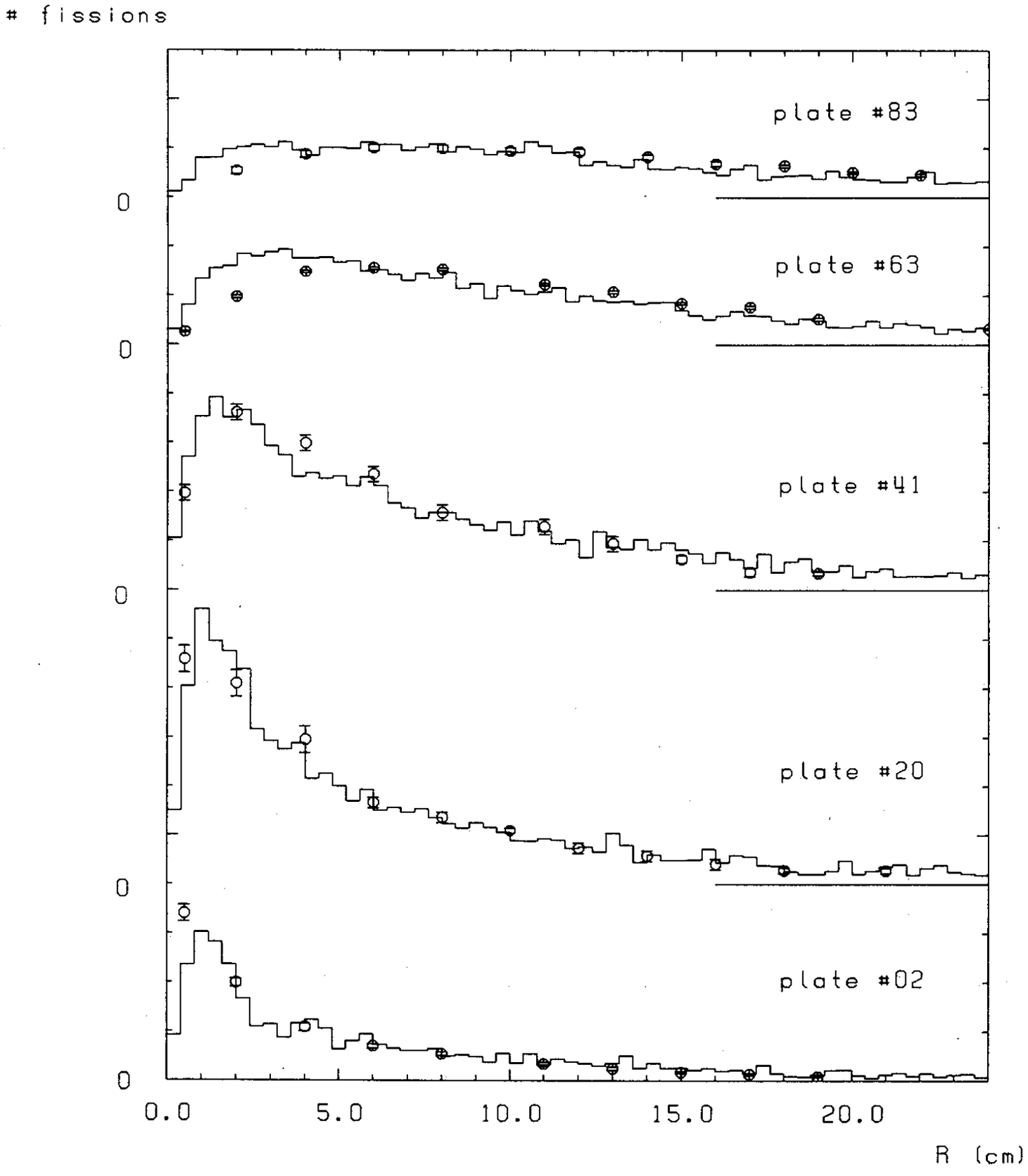

Fig.13 As in fig.12 but for the fission products;

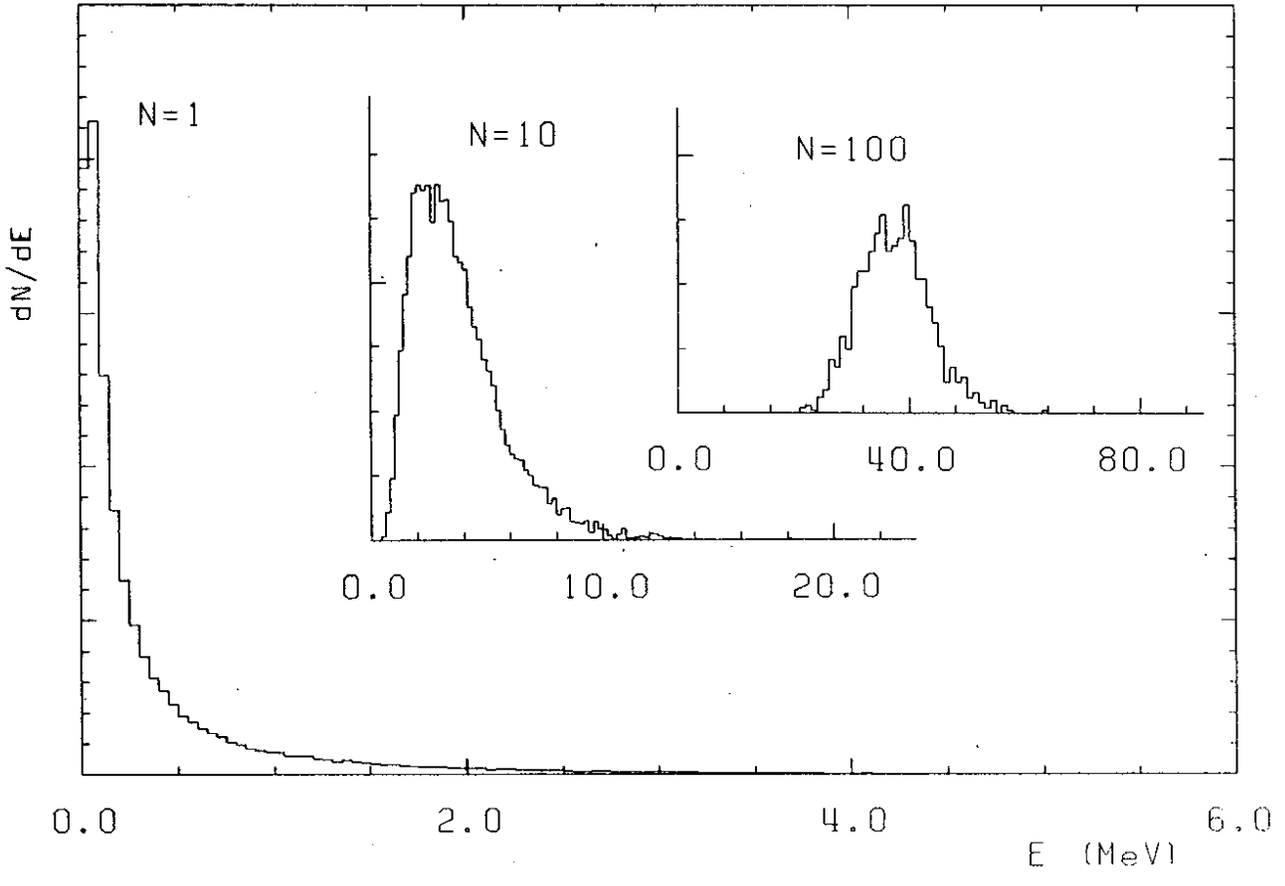

Fig.14 The signal E of a single neutron and the signal created by a group of N-neutrons (in arbitrary units) for N=10 and 100.

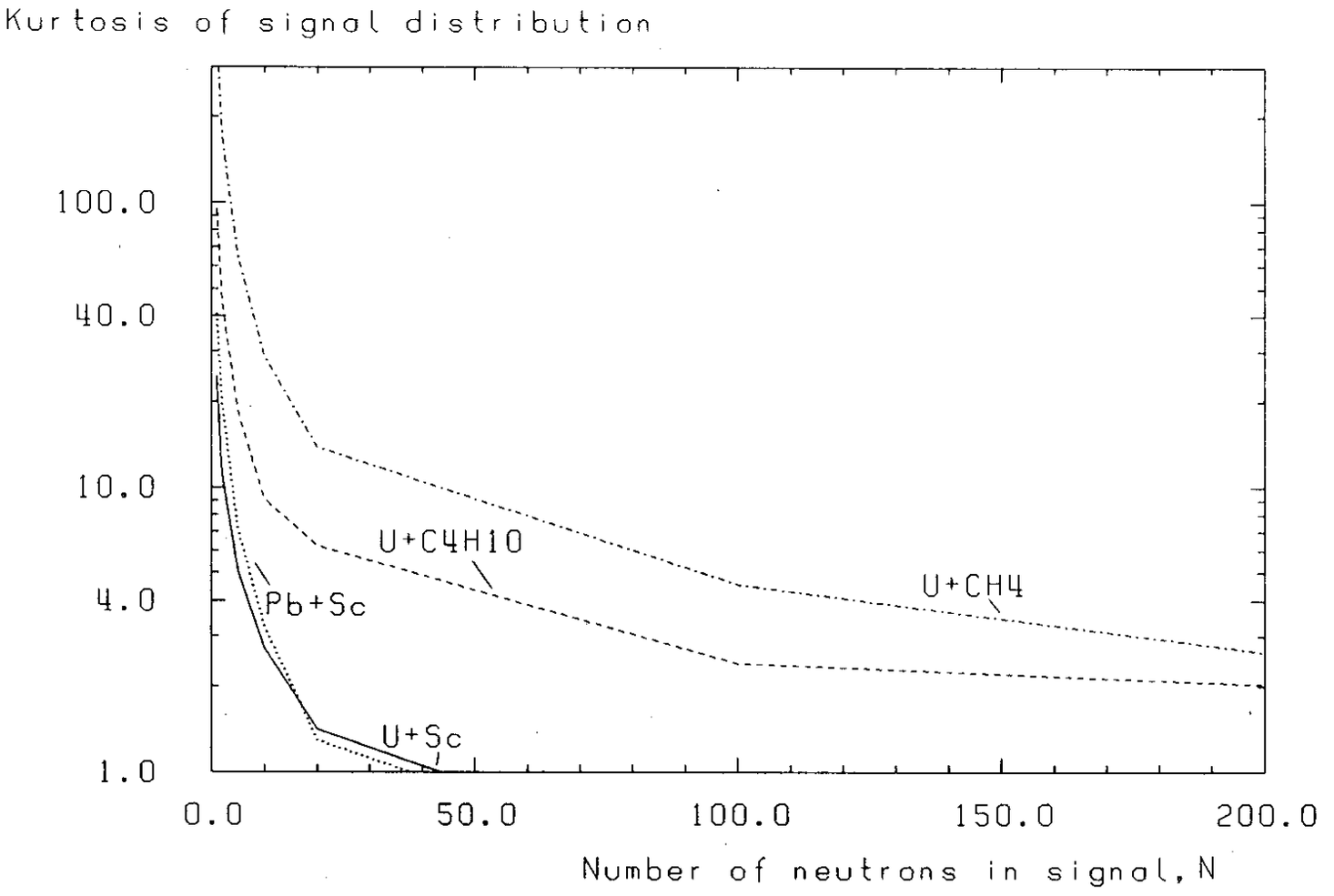

Fig.15 The kurtosis of neutron signal distributions in a uranium compensating calorimeter(full line), the lead compensating calorimeter(dotted line) and the gas-uranium calorimeters (methane – dashed-dotted line, isobutane – dashed line) as a function of number of neutrons,N, creating the signal. It is expected to be zero for a Gaussian distribution.

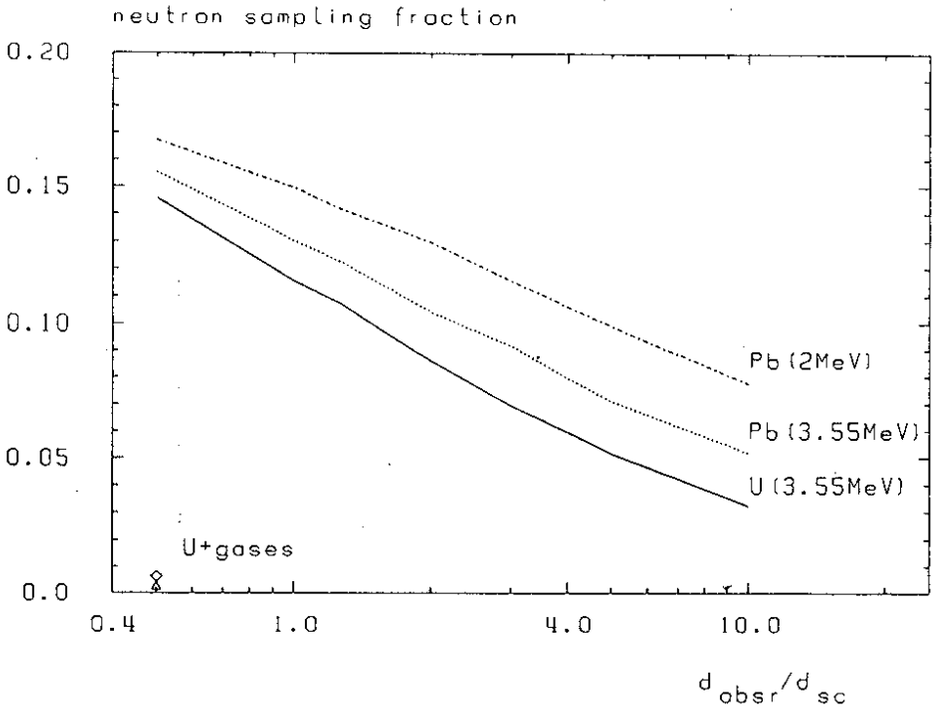

Fig. 16 a

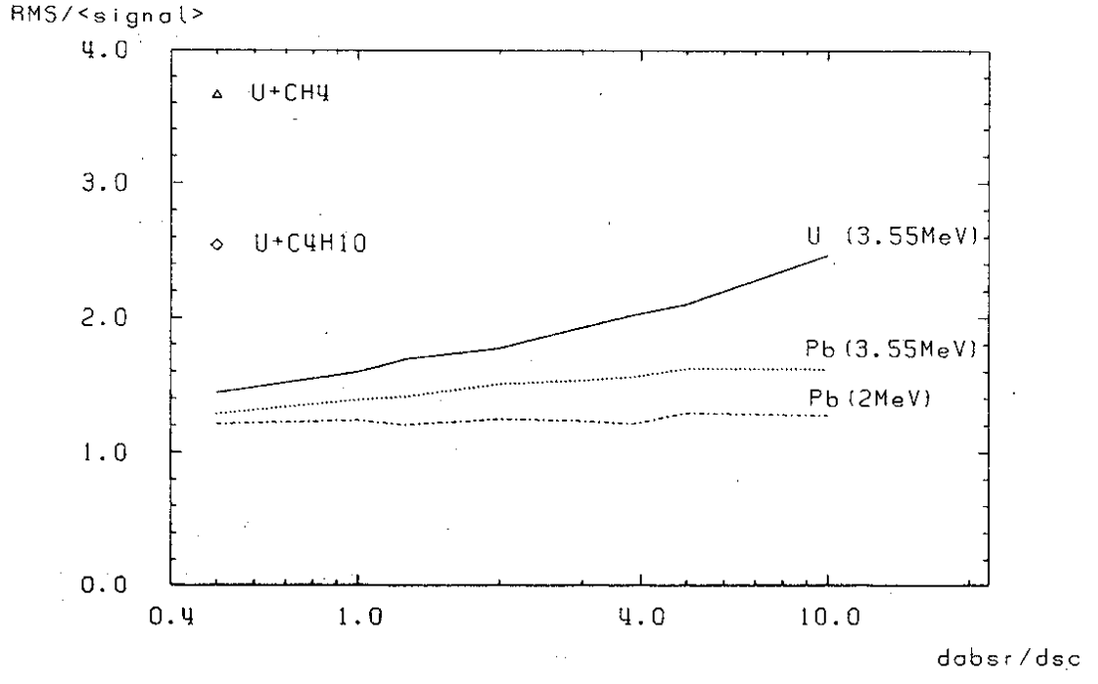

Fig. 16 b

Fig.16 The neutron sampling fraction α_n (a), and the one neutron resolution, $\sigma_{1n}^{signal} / < signal >_{1n}$, (b), as a function of the ratio of thicknesses of absorber and scintillator, d_{absr}/d_{Sc}, per evaporation neutron for uranium and lead calorimeters. For lead the calculations are done for mean neutron energies of 3.55 MeV and 2 MeV(see sect.2). A scintillator thickness of 0.26 cm is taken for all the calculations. For a visual comparison the results of gas-uranium calorimeters are added and placed at d_{absr}/d_{Sc}=(0.33cm/0.66cm)=0.5 as squares for isobutane and as triangles for methane. It should be scaled as $(d_U/\Lambda_U)/(d_{readout}/\Lambda_{readout})$, but it leads to an unclear graph.

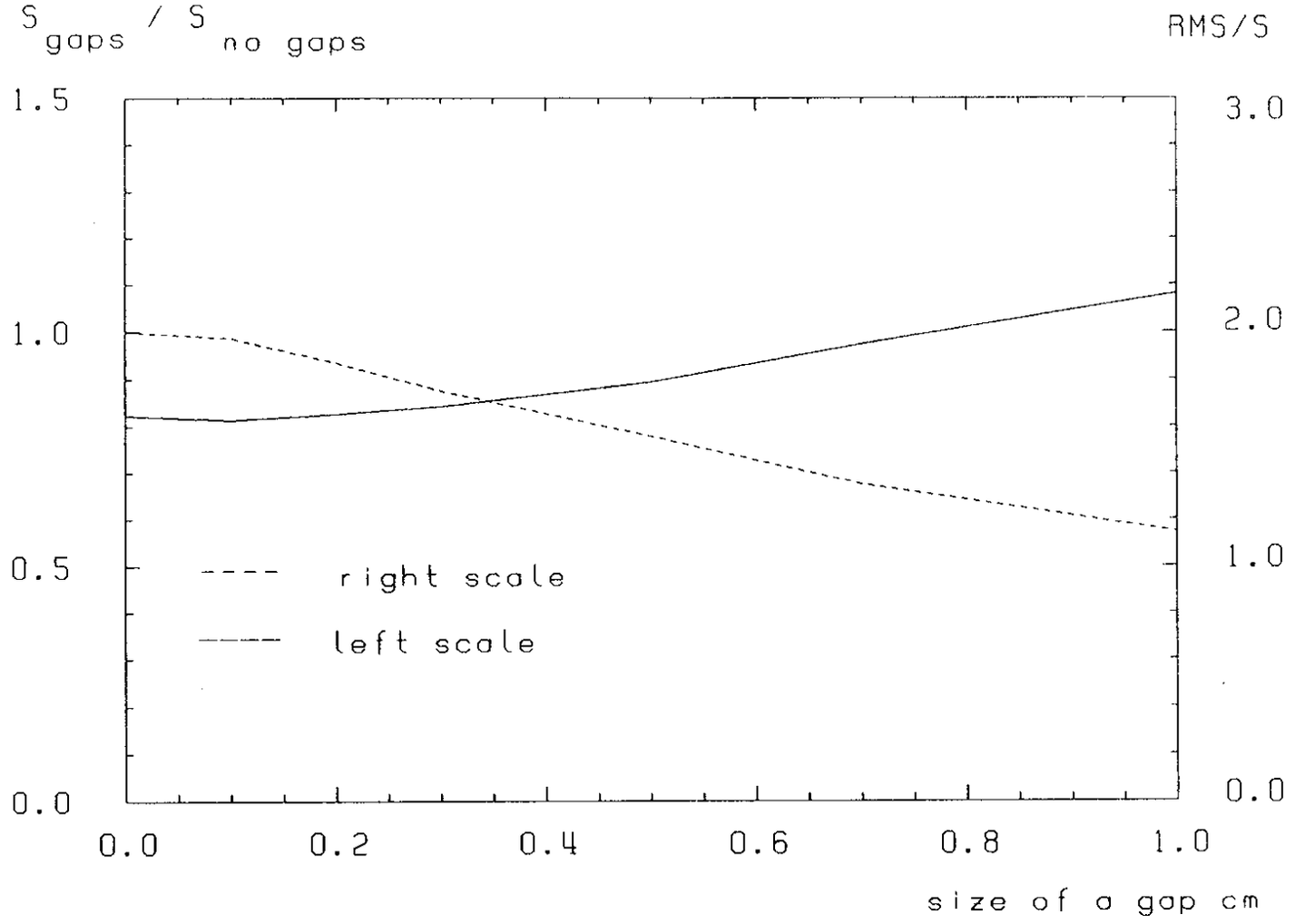

Fig.17 The fraction of the detected neutron signal S (dashed line) and the resolution (full line) as a function of the size of gaps inside the uranium compensating calorimeter.

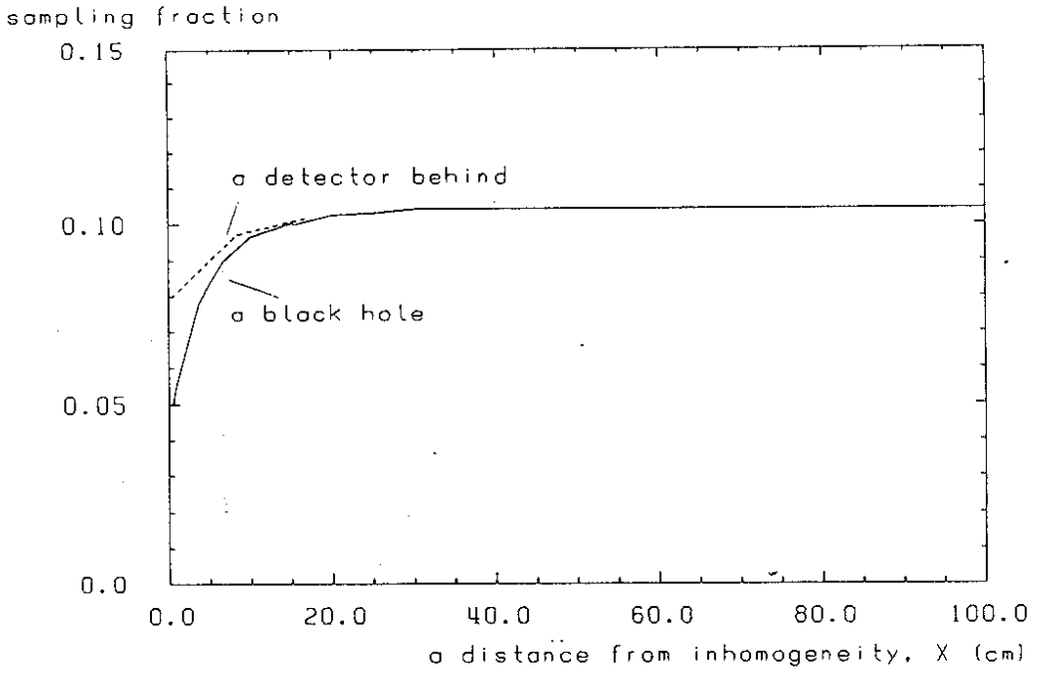

Fig. 18 a

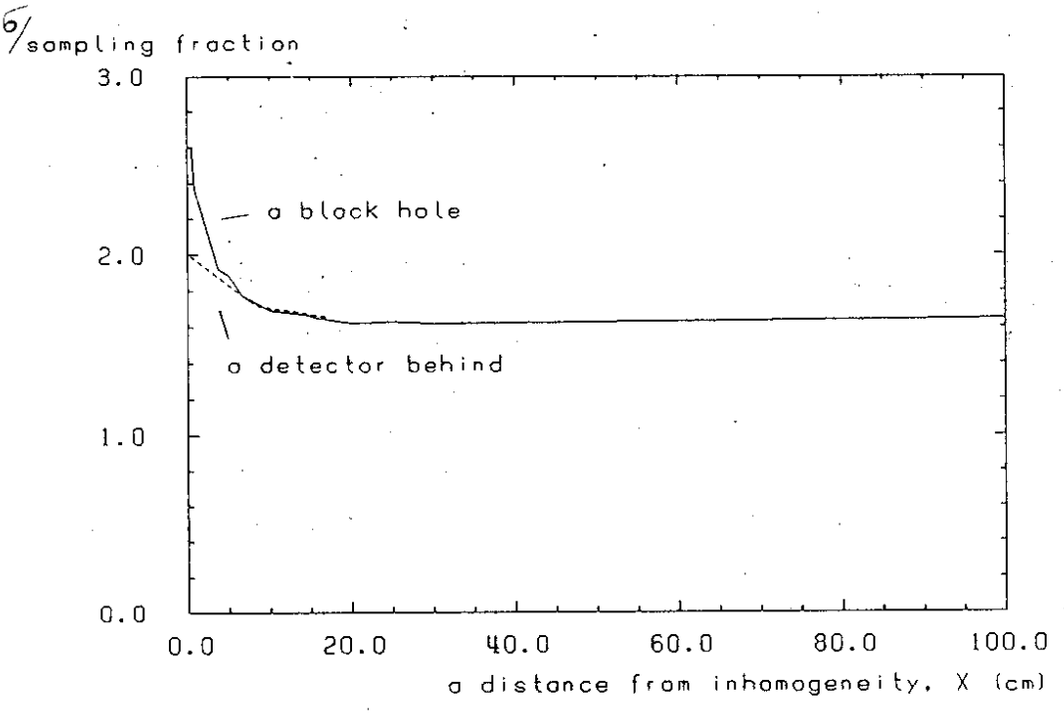

Fig. 18 b

Fig.18 Studies of the effects of inhomogeneity in calorimeter geometry (a front wall, dead material, limited transversal size of a calorimeter); this figure presents the neutron sampling fraction (a) and neutron resolution (b) calculated as a function of the distance X of the evaporation neutron source from inhomogeneous point for the uranium compensating calorimeter. The dashed line — if another detector is nearby, here at a distance of 10 cm.